# *Synthetic mRNA Delivery Platform for Ex Vivo Transfection of Natural Killer Cells*

## Polymer- and Lipid Nanoparticle-based mRNA Delivery Vehicles to Optimize Natural Killer Cells for Adoptive Cell Therapy

Lisa Brandenburg

6151825 | Major Research Project | MSc Drug Innovation (Utrecht University)

| | |
|---|---|
| Daily supervisor | Stefania Douka |
| First Examiner | Dr. Massimiliano Caiazzo |
| Second Examiner | Prof. Dr. Enrico Mastrobattista |

January 2023

# Table of Content

# Abbreviations

| | |
|---|---|
| ACT | Adoptive Cell Therapy |
| ADCC | Antibody-dependent cell-mediated cytotoxicity |
| AIBN | Azobisisobutyronitrile |
| AzEMAm | 2-azidoethylmethyacryl-amide |
| BAP | 1,4-bis(3-amino propyl)piperazine |
| bis5F | Bis(pentafluorophenyl) carbonate |
| CRS | Cytokine Release Syndromw |
| DLS | Dynamic Light Scattering |
| DMG-2kPEG | 1,2-dimyristoyl-sn-glycerol methoxypolyethylene glycol |
| DSPC | 1,2-distearoyl-sn-glycero-3-phosphocholine |
| DTDE | 1,4-Bis(sulfanyl)butane-2,3-diol |
| DTDE-bis5F | 2,2-bisulfanediylbis(ethane-2,1-diyl) bis(pentafluorophenyl) bis(carbonate) |
| EE% | Encapsulation Efficiency percentage |
| eGFP | enhanced Green Fluorescent Protein |
| GPC | Gel permeation chromatography |
| GVHD | Graft-versus-Host Disease |
| LNP | Lipid Nanoparticle |
| MFI | Mean Fluorescent Intensity |
| N/P ratio | Nitrogen to Phosphorus ratio |
| NK cell | Natural Killer cell |
| $P_5D_{39}$ | PEG5K-pDMAEMA39K |
| PDI | Polydispersity index |
| pDMAEMA | poly(2-(dimethylamino)ethyl methacrylate) |
| pDNA | plasmid DNA |
| PDTEMA | N-[2-(2-pyridyldithio)]ethyl methacrylamide |
| PEG | Polyethylene glycol |
| PEI | Polyethyleneimine |
| pHDePA | poly(HPMA-DEAE-co-PDTEMA-co-AzEMAm) |
| pHPMA-DEAE ester) | poly(Carbonic acid 2-diethylamino-ethyl ester 1-methyl-2-(2-methacryloylamino)-ethyl |
| PUBAP | BAP-residue-containing polyurethane |

# Abstract

Natural Killer (NK) cells are a promising approach for adoptive cell therapy (ACT) since they can initiate a strong cytotoxic anti-tumor response, as the result of a balanced interplay between activating and inhibiting receptors. Although NK cells are considered less toxic and possibly also more effective than T cells, making them a potent alternative for immunotherapy, clinical efficacy of NK cells may be limited due to a lack of solid tumour infiltration and tumour editing causing suppression of NK cytotoxicity. These issues may be overcome by optimizing the cellular phenotype with additional activating receptors or silencing inhibitory receptors, through genetic manipulation. Yet, current methods for gene transfection of NK cells are lacking in efficiency or they induce undesired toxicity or phenotypical changes in the cells. A well-characterized nonviral method for NK cell transfection is thus desired. Towards this end, this research describes the synthesis of cationic polyplexes and lipid nanoparticles (LNPs) for the efficient delivery of enhanced Green Fluorescent Protein (eGFP) mRNA to NK cells. Although positively charged mRNA-polyplexes were unsuccessful for NK cell transfection, even when combined with cellular uptake and endosomal escape enhancing peptides, LNPs proved to be a suitable mRNA delivery platform. Upon optimization of the LNP lipid composition, including the use of Lipid 5 as ionizable lipid and $\beta$-sitosterol (instead of cholesterol) as steroid, as well as microfluidics optimization, transfection efficiency up to ~85% eGFP expression was reported for the KHYG-1 NK cell line. Ultimately, the optimized LNP formulation presented ~75% transfection efficiency in umbilical cord blood derived NK cells, with a 5.5-fold increase in fluorescence from eGFP expression compared to the next-best nonviral alternative for NK cell transfection, electroporation. The reported LNP formulation is an effective non-toxic method for gene delivery in clinically relevant NK cells and may thus provide a suitable platform of phenotypical NK cell optimization for adoptive cancer immunotherapy.

## Layman Summary

Immunotherapy is a type of cancer treatment in which an infusion of immune cells is administered to help fight tumor cells. Currently, T cells are being used for this application, but Natural Killer (NK) cells are becoming a promising alternative. Being part of the innate immune system, NK cells are able to initiate a strong immune response against cancerous tissue. The anti-cancer activity of T cells is dependent on tumors expressing recognizable receptors on their surface, but cancerous tissue can inhibit the expression of these surface receptors, thus inactivating the T cells response. Meanwhile, NK cells can still attack tumor cells as they are not reliant on the recognition of these surface markers. Moreover, NK cells are less likely to attack healthy tissue, and thus considered safer than T cells for immunotherapy. Although they pose a promising candidate, NK cells may lack clinical efficacy as they can fail to permeate solid tumors and their immune response is frequently downregulated in the cancer environment due to tumor-released cytokines. Genetic manipulation of NK cells, by which activating receptors are enhanced through the delivery of mRNA into the cytosol, could provide a solution for these issues. However, intracellular gene delivery poses a challenge, especially in NK cells, as mRNA cannot be taken up by the cell directly. A delivery vehicle, in which the mRNA is encapsulated, must be used, yet current approaches which are based on electroporation or viral methods are either lacking efficient delivery in NK cells or causing unwanted changes in the cell phenotype. Hence, an alternative delivery vehicle is required. Accordingly, this research proposes the use of polymer- or lipid-based particles as delivery platforms for mRNA, described as polyplexes or lipid nanoparticles (LNPs), respectively. Polyplexes are prepared from cationic polymers that make a complex with the anionic mRNA through electrostatic interactions, thus forming a cationic particle with a diameter in the nanometer range. LNPs are mainly composed of an ionizable lipid which is neutral at a physiological pH but becomes cationic in an acidic environment and thus allows for similar electrostatic complexation with mRNA. Combined with various helper lipids, LNPs fully encapsulate the mRNA and generate a slightly negatively charged particle in physiological conditions. This research showed no successful mRNA delivery via polyplexes from various polymers, nor did delivery improve when peptides were added that should stimulate cellular uptake of the particles and subsequent mRNA release into the cytosol. However, LNPs proved to be an effective method and optimization of the lipid composition and formulation parameters resulted in an mRNA delivery of 85%. This percentage minorly decreased to 75% in clinically relevant primary NK cells, which is still significantly higher than the currently used alternative for mRNA delivery in NK cells, which is electroporation. Thus, the optimized LNP formulation poses a promising approach for genetic manipulation of NK cells for immunotherapy.

# 1. Introduction

Immunotherapy is a vastly emerging field in oncology, providing treatment options for many cancer types. Although immune checkpoint inhibitors and targeted therapy with monoclonal antibodies have shown to greatly improve survival rates in treatment-resistant and metastatic tumor types, their therapeutic response is commonly short-lived and comes with a substantial risk for both acute and long-term toxicity issues[1–3]. Adoptive cell therapy (ACT) is a highly promising alternative in which patients intravenously receive expanded and/or genetically modified immune cells to enhance the anti-tumor effect. Thus far only T cells are clinically approved for this purpose, yet natural killer (NK) cells have shown to also be a successful candidate in early clinical trials[4,5].

Unlike T cells, NK cells are part of the innate immune system, and hence do not require prior immunization with a tumor-specific antigen to induce direct cell killing and rapid release of pro-inflammatory cytokines[6,7]. Their cytotoxicity is generated via the exocytosis of lytic granules, such as granzyme B and perforin, or by direct receptor-mediated apoptosis (through Fas ligand and TNF-related apoptosis-inducing ligand expression on NK cells)[5,8]. These immune responses are either induced or suppressed as a result of a balanced interplay of activating and inhibitory receptors across the NK cell surface. CD16 is herein the most potent activating receptor, as it interacts with the Fc region of opsonized IgG antibodies, upon which it initiates antibody-dependent cell-mediated cytotoxicity (ADCC)[9,10]. Unlike other NK cell receptors, CD16 can induce apoptosis without requiring additional stimulating signals from other receptors[10,11]. This ADCC pathway opens the possibility of NK cell therapy combined with currently available tumor-targeting monoclonal antibodies for an enhanced dual treatment[12]. CD16 is highly expressed in the most predominant NK cell subset in peripheral blood, CD56^{dim} NK cells. Hence, this NK cell subset is more involved in direct cell-mediated cytotoxicity. CD56^{bright} cells present low CD16 expression and are generally weakly cytotoxic (unless activated by IL-15), yet they efficiently produce IFNγ, TNF and other cytokines[9,11]. Not only do these pro-inflammatory cytokines enhance the cytotoxic T cell response, but they also exert potent anti-proliferative, anti-angiogenic, and pro-apoptotic effects on cancer cells[5,13].

Besides CD16, NK cells present a variety of activating receptors, including NKp30, NKp44, NKp46, NKG2C and NKG2D, which recognize viral, bacterial and/or tumor-associated ligands on infected or transformed cells. NKG2D plays a key role in anti-tumor activity, as it binds to MHC class I chain-related molecules (MICA/B) and the RAET1/ULBP family of proteins, which are expressed on a broad range of tumor cells but only poorly expressed in healthy cells[14–16]. Moreover, tumorigenesis results in upregulation of MICA/B and ULBPs through stress pathways[17]. NKp30 and NKp44 recognize highly tumor-specific ligands such as B7-H6[18] and BAT-3[19] (ligands for NKp30), and Nidogen-1[20], proliferating cell nuclear antigen[21] and 21spe-MML5[22] (ligands for NKp44). Besides direct interaction with cancer cells, NK cells can also exert cytotoxic functions upon chemokine interactions with its chemotactic receptors, CXCR3–CXCR4, CX3CR1 and CCR3–CCR5[5,23].

NK cells also possess a repertoire of inhibitory receptors, NKG2A and the killer immunoglobulin-like receptor (KIR) family, to counteract stimulatory signals. These receptors interact with class I HLA molecules (HLA-A, HLA-B, HLA-C, HLA-E and HLA-G) to intracellularly reduce downstream signaling and thereby dampen the immune response[24,25]. NKG2A is considered the major inhibitory receptor and forms a compelling therapeutic target for blockage as both the receptor and its ligand (HLA-E) are non-polymorphic[25]. The KIR family consists of 14 receptors which can be divided into activating and inhibitory types, based on the presence of a short or long intracellular tail on the activating domain, respectively[24,26]. One exception is KIR2DL4, carrying both activating and inhibitory functions[26]. Inhibiting receptors are a crucial part of anti-tumor immunity through the "missing-self response": cancer cells frequently

downregulate HLA molecules to evade T cell recognition, yet this lack of inhibitory signaling via KIR receptors causes the NK cells to activate and initiate an immune response[27]. This mechanism forms one of the major therapeutic benefits of NK cell-based ACT compared to the current use of T cells.

Cancer cells, especially solid tumors, are known to downregulate or modulate antigens to the point where T cells are unable to induce a sufficient immune response[28]. As a result, chimeric antigen receptor (CAR)-based T cell therapies demonstrate a high posttherapy relapse rate due to acquired resistance[29]. NK cells would in this case still be able to respond through lack of inhibitory signals and remaining stimulating ligands on the tumor surface[6,7]. Furthermore, T cell ACT presents serious toxicity risks through on-target off-tumor effects (due to biomarker presence on healthy tissues)[30], graft-versus-host disease (GVHD) (from allogeneic CAR-T cells)[31] and cytokine release syndromes (CRS)[32]. NK cells, on the other hand, clinically rarely cause GVHD and may even have a protective effect[33–36]. Compared to CAR-T cells, there is no evidence of CRS, neurotoxicity or GVHD upon NK cell administration for hematological malignancies[33–37]. Moreover, T cell ACT is typically only available from autologous cells to mitigate toxicity risks, requiring a costly and complex manufacturing process with a treatment delay of approximately 3 weeks for each patient[31]. By not requiring HLA-matching, allogeneic NK cells become more accessible, creating the possibility for an "off-the-shelf" product. A notable example of such off-the-shelf, more broadly compatible, allogeneic cells are $CD34^+$ umbilical cord blood-derived progenitor NK cells, which are currently being evaluated in Phase II clinical trials[38].

However, the main challenge of NK cells arises as they are hard-to-transfect cells and hence are not easily genetically reprogrammed[39,40]. Genetic engineering is required to optimize the NK cell phenotype for ACT, as it prevents immune suppression by the tumor microenvironment and enhances (solid) tumor infiltration through upregulation of activating receptors[39,41] (Figure 1). Viral transduction is commonly applied for this purpose, yet the overall efficiency is relatively low, possibly due to the strong antiviral mechanisms of NK cells[42,43]. Although some retroviruses-based methods report transduction efficiency up to 70%, cell viability and the need for repeated transduction rounds remains an issue[43]. Moreover, viral methods carry the risk for insertional mutagenesis, come with immunogenicity-related regulatory issues and high production costs due to the need for high-biosafety laboratories[40,43]. Lipofection, in which nucleic acids are encapsulated by cationic liposomes, is an upcoming viral free alternative in NK cell modification, yet it generally presents low transfection efficiency[42]. Electroporation with messenger RNA (mRNA) is currently the most common non-viral approach for genetic manipulation of primary NK cells[43], but the harsh transfection conditions result in low cell viability[40] and may cause phenotypical changes leading to loss of initial NK cell characteristics[44,45].

Ultimately, there is still a need for a transfection method that is not only efficient and well-tolerated in primary NK cells, but also well-characterized to allow for a clinical application in ACT. To this end, nanoparticles are a suitable platform for nucleic acid delivery, with clinical applications already worldwide[46,47]. However, these approved applications are limited to gene therapies and vaccines[46], and the question remains whether they can also be used in adoptive cell therapy, especially regarding NK cells. Nanoparticles for nucleic acid delivery can be divided into three main categories: polymeric, lipid-based and inorganic nanoparticles. The latter of these finds its main application in theranostics and is generally associated with high toxicity and low solubility due to the use of nonbiodegradable materials[46]. Hence, this research is limited to polyplexes and lipid nanoparticles (LNPs) as mRNA delivery vehicles for primary NK cells.
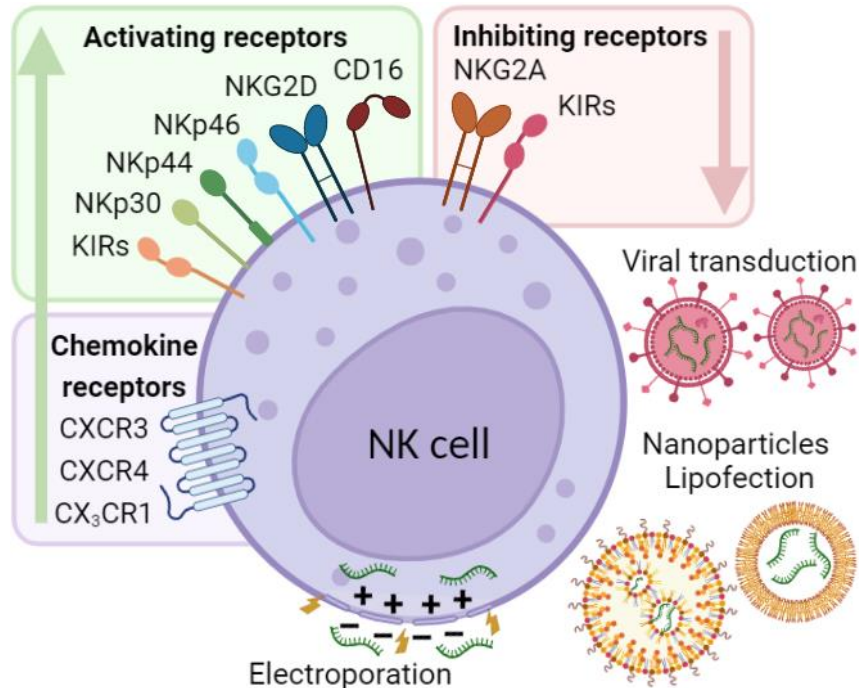
*Figure 1. Methods for genetic engineering of NK cells for an improved ACT phenotype. Green arrow indicates the possibility for receptor upregulation (i.e., via gene delivery with presented transfection methods). Red arrow indicates the possibility for receptor downregulation (i.e., gene knockout or silencing RNA delivery).*

Polyplexes are interpolyelectrolyte complexes which are formed through electrostatic interactions between cationic polymers and the anionic nucleic acid cargo[48]. The wide availability of cationic polymers, ranging from polypeptides such as poly(lysine) to nondegradable polymers like polyethylenimine (PEI), allows for a variety of characteristics that can be fine-tuned for each application[46,48,49]. Although these particles are highly adaptable, it should be noted that polyplexes generally carry a relatively high positive surface charge (due to the cationic nature of the polymers), which is commonly associated with higher cellular uptake yet also greater cytotoxicity than neutral particles[50]. Recently, a biodegradable core-shell mRNA-polyplex with surface functionalization was developed within our department, which showed successful transfection of dendritic cells[49,51]. This nanoparticle uses a methacrylamide triblock co-polymer (referred as pHDPA), consisting of a biodegradable cationic residue (HPMA-DMAE), a disulfide-based crosslinking monomer (PDTEMA), and an azide-carrying moiety for click chemistry (AzEMAm). Whilst the cationic amine complexates with mRNA, the cross-linking monomer allows for stabilization of the polyplex, and the azide subsequently enables addition of specific targeting peptides or a polyethylene glycol (PEG) coating[49]. Inspired by its successful mRNA transfection in dendritic cells, a similar approach was hypothesized for NK cell transfection. Previous research by Luten et al has shown that methacrylamide polymers with diethyl amino side chains generally result in higher transfection efficiency than its analogues with a dimethyl amino group[52]. Hence, in our research the trimeric polymer is designed to contain a dimethyl-based cationic monomer (HPMA-DEAE), resulting in the triblock co-polymer p(HPMA-DEAE-*co*-PDTEMA-*co*-AzEMAm) (further denoted as pHDePA, Figure 3A). Since this redesigned polyplex is aimed for *ex vivo* application, a PEG coating (normally added for prolonged systemic circulation of nanoparticles) and NK targeting peptides are not deemed necessary as additional surface modifications. Hence, the azide functionality may be used for other purposes. As endosomal escape is commonly recognized as the bottleneck of nucleic acid delivery via nanoparticle systems[48,53], endosomal escape-facilitating peptides may also be added to enhance the transfection efficiency.

Lipid-based nanoparticles have rapidly gained attention as nucleic acid delivery platform through their global introduction as part of the COVID-19 vaccines[47,54,55]. Being the first clinically approved mRNA-LNPs, they illustrate the potential of similar formulations for other applications, such as NK cell ACT. LNPs mainly consist of a pH-sensitive ionizable lipid, which is neutral in physiological conditions, but becomes protonated in acidic environments where it consequently engages in electrostatic interactions with nucleic acids[56,57]. Additionally, various helper lipids are required to form a stable particle; phospholipids to form a particle membrane, cholesterol for membrane stabilization and PEGylated lipids for stability and solubility[46,56]. Together, this typically results in near-neutrally charged spherical particles, ranging between 50 and 150 nm in diameter, with micellar structures within the LNP core (Figure 2)[46,58]. Although slightly less adaptable than polyplexes, LNP characteristics can be altered through changes in the lipid composition and formulation parameters[58]. Besides particle complexation, the ionizable lipid also aids in endosomal escape as it becomes cationic in the acidic endosome and can thus insert its cationic lipid tails into the endosomal membrane[59,60]. As a starting point for mRNA-LNP transfection of NK cells, the ionizable lipids SM-102 and Lipid-5 were used during a preliminary screening.
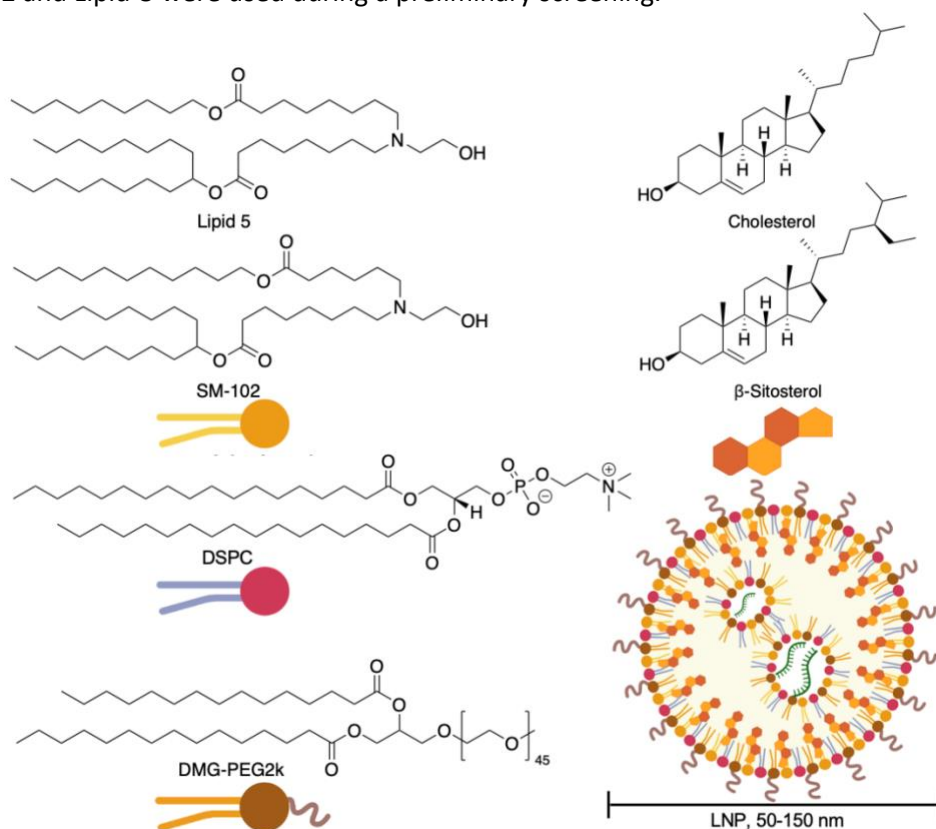


*Figure 2. LNP composition.*

Towards a solution for the current lack of efficient genetic engineering in NK cells, the aim of this research was to find a well-characterized delivery platform for *ex vivo* mRNA transfection of umbilical cord blood-derived primary NK cells using polymer and lipid-based nanoparticles.

# 2. Results & Discussion: Polymeric Particles

## 2.1 Preparation & Characterization of mRNA-Polyplexes

To study the efficacy of mRNA-containing polyplexes in NK cells, various cationic polymers were synthesized. The random triblock co-polymer p(HPMA-DEAE-*co*-PDTEMA-*co*-AzEMAm) (pHDePA) and its corresponding homopolymer, pHPMA-DEAE, were synthesized via free radical polymerization (Figure 3A, Scheme S1, Scheme S2). The cationic polyurethane containing multiple disulfide and 1,4-bis(3-aminopropyl)piperazine (BAP) residues (PUBAP) was prepared by polycondensation between 2,2'disulfanediylbis(ethane-2,1-diyl) bis(pentafluorophenyl) bis(carbonate) (DTDE-bis5F) and BAP (Figure 3A, Scheme S3). The synthesized polymers, as well as PEG-pDMAEMA ($P_5D_{39}$), were characterized for their composition (by $^1$H NMR) (Figure S1-S3) and molecular weight (by GPC). These characteristics are summarized in Table 1, presenting molecular weights of ~20 kDa, similar to previously reported syntheses[51,52], with the exception of PUBAP. According to literature, a comparable molecular weight of 20 kDa is to be expected for PUBAP[61], yet the synthesized product is notably shorter around 4 kDa. The reduction in polymer length can likely be attributed to an inaccurate 1:1 ratio between DTDE-bis5F and BAP during polymerization, due to the presence of bis(pentafluorophenyl) carbonate remaining from the activation of DTDE-bis5F (Figure S4). The residual bis(pentafluorophenyl) partially consumes the BAP, causing the DTDE-bis5F:BAP ratio to deviate further. Although the molecular weight was considerably lower than expected, the PDI was comparable to literature[61], and agarose retardation assay showed successful complexation of the PUBAP with mRNA, hence the polymer was used for further experiments.

*Table 1. Polymer characterization.*

| Polymer | Mn[a] (kDa) | PDI[a] | HPMA-DEAE/PDTEMA/AzEMAm Ratio[b] |
|---|---|---|---|
| $P_5D_{39}$ | 27 | 2.3 | - |
| pHPMA-DEAE | 21 | 4.7 | - |
| pHDePA | 18 | 1.7 | 52/22/26 |
| PUBAP | 3.5 | 1.6 | - |

[a]Determined by GPC. [b]Determined by $^1$H NMR.

Polyplexes were prepared through self-assembly via electrostatic interactions between the cationic amine-carrying polymers and the anionic phosphate residues in the mRNA. To determine the optimal amine to phosphate molar ratio (N/P) required for complexation, agarose gel retardation analysis was performed for each polymer. The addition of anionic heparin to these polyplexes shows the possibility of complexation reversibility and mRNA release (Figure 3B). Besides the minimally required N/P ratio, higher N/P ratios were in some cases also prepared to obtain smaller particles via more compact complexation as a result of polymer surplus. Whilst these smaller particles should facilitate more rapid cellular uptake, the cationic polymer excess allows for increased cell penetration and endosomal escape[61–63]. However, the presence of free cationic polymer is typically accompanied by higher toxicity and should thus be carefully balanced. The obtained particles were characterized by size, polydispersity and zeta-potential, as presented in Table 2. This shows the formation of overall highly cationic monodisperse particles, mostly with sizes varying around 150 nm in diameter. Only the $P_5D_{39}$ forms smaller particles with a diameter <100 nm, which allows for studying the effect of size on the transfection efficiency in NK cells. The expected decrease in size upon an increase in N/P ratio is illustrated by pHDePA, dropping from 221 nm to 164 nm by doubling the N/P ratio. Overall, the characteristics of the cationic polyplexes are in line with those reported in literature[51,52,64]. Surprisingly, the PUBAP-mRNA polyplex carries a negative zeta-potential, although the polymer itself was shown to be strongly cationic when measured by Zetasizer as free polymer (Table S1). This is possibly due to its relatively low N/P ratio compared to literature[61].

Table 2. Polyplex characterization.

| Polyplex | N/P ratio | Size$^a$ (nm ± SD) | PDI$^a$ | ζ-potential$^b$ (mV ± SD) |
|---|---|---|---|---|
| PEI | 40 | 138 ± 1.15 | 0.23 | +17.5 ± 2.2 |
| P$_5$D$_{39}$ | 15 | 77 ± 0.33 | 0.22 | +13.0 ± 1.4 |
| pHPMA-DEAE | 5 | 185 ± 3.04 | 0.33 | +20.1 ± 0.26 |
|  | 10 | 263 ± 288$^c$ | 0.57$^c$ | NT$^c$ |
| pHDePA | 5 | 221 ± 3.27 | 0.20 | +17.8 ± 0.17 |
|  | 10 | 164 ± 3.05 | 0.21 | +14.3 ± 0.32 |
| PUBAP | 5 | 148 ± 8.65 | 0.28 | -14.2 ± 0.72 |

$^a$Determined by DLS. $^b$Determined by Zetasizer. $^c$Error due to contamination.
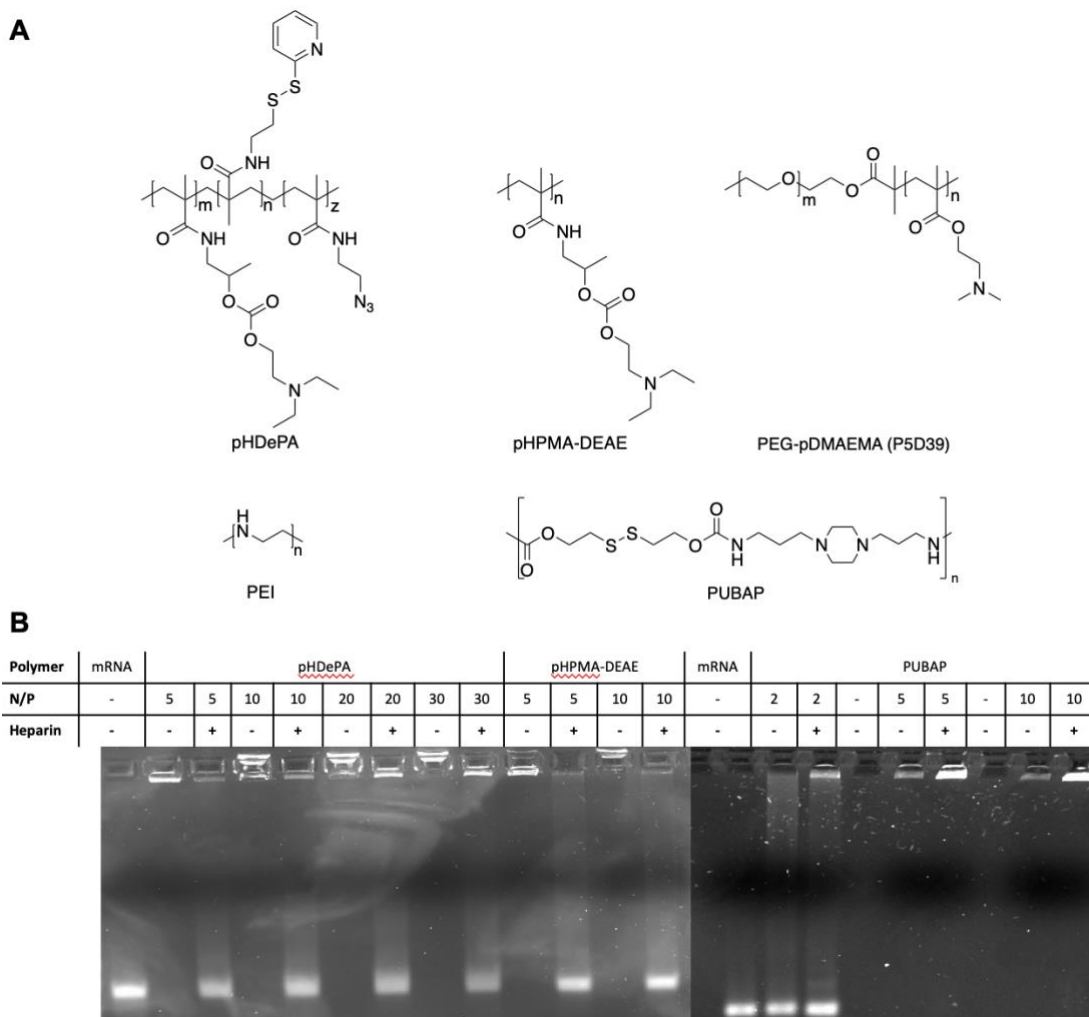


Figure 3. (**A**) Structures of all polymers used. (**B**) mRNA-polyplex complexation visualized by agarose retardation assay. Heparin had likely degraded in PUBAP samples, thus not showing mRNA release from the polyplex.

## 2.2 mRNA-Polyplexes Fail to Transfect HEK 293T & NK Cells

Transfection assays were carried out with enhanced Green Fluorescent Protein (eGFP) encoding mRNA in two types of immortalized NK cells lines, KHYG-1[65] and NK-92[66], as well as a control cell line of human embryonic kidney (HEK 293T) cells. The two NK cells lines were used to provide a sustainable model of the transfection response in primary NK cells. In the case of HEK 293T cells, the 24-hour incubation period with polyplexes was carried out in serum-free medium, as the presence of serum supposedly decreases transfection efficiencies by serum albumin-induced prevention of polyplex aggregation and subsequent sedimentation of the particles on the attached cells[67,68]. In contrast, both NK cells lines are suspension cells, hence sedimentation of the particles on their surface is not part of the polyplex uptake mechanism and cells could thus be cultured in serum-supplemented medium for increased viability.

For the transfection experiments commercial transfection reagents Lipofectamine[TM] 3000 and Lipofectamine[TM] LTX were used as positive controls. According to Figure 4, only PUBAP-mRNA polyplexes showed eGFP expression in HEK 293T cells, with an average of 6% transfected cells (Figure 4A). The cationic polyplexes, did not successfully induce eGFP expression in HEK 293T cells. Similarly, no transfection could be observed with any of the polyplexes in both NK cell lines (Figure 4B&C). The lack of NK cell transfection by commercial reagents (i.e., Lipofectamine[TM] LTX) is in line with previous research[44]. Deficient mRNA delivery in NK cells could possibly be attributed to the strongly positive zeta-potential of the polyplexes, comparable to the Lipofectamine[TM] reagents, which seemingly is not a successful approach for NK cell transfection. Although endosomal escape is frequently considered the bottleneck of gene delivery, the highly cationic nature of these particles should overcome this obstacle[53]. Alternatively, the uptake of such cationic polyplexes may not be favored by NK cells, causing the ultimately lack of mRNA delivery to the cytosol. Overall, toxicity of these particles does not seem to be an issue; viability of all cell types is >95%, with the exception of $P_5D_{39}$, which is not biodegradable unlike the other polymers and may therefore accumulate, thus inducing toxicity.
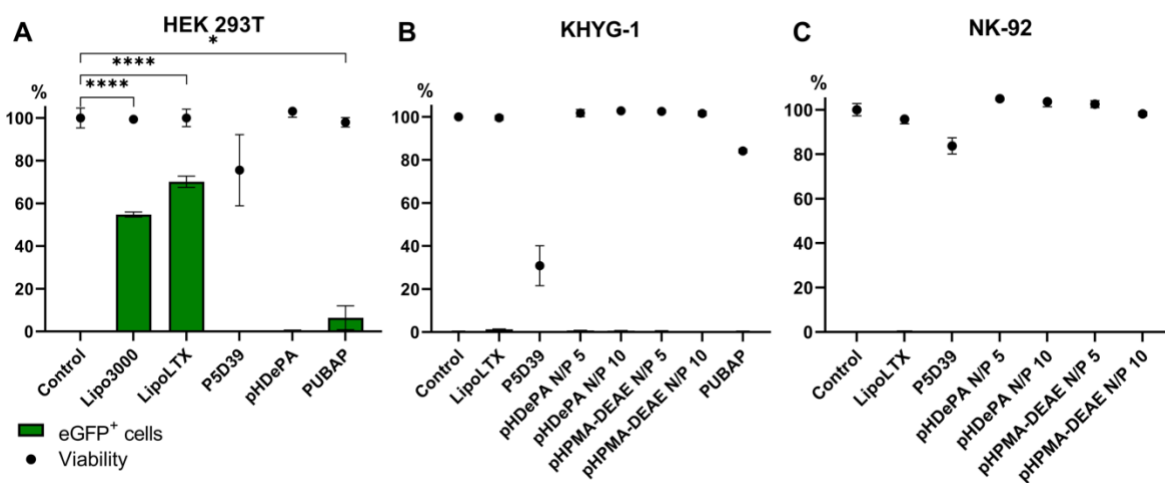


*Figure 4. Polyplex transfections in (**A**) HEK 293T, (**B**) KHYG-1 and (**C**) NK-92 cells. In HEK 293T, pHDePA-based polyplexes were applied at N/P 10. \*p<0.05, \*\*\*\*p<0.0001.*

## 2.3 Cell Penetrating & Endosomal Escape Peptides Do Not Induce mRNA-Polyplex-based Transfection of KHYG-1 & HEK 293T cells

With little to no transfection in HEK 293T and NK cells, and the lack of polyplex uptake as a possible explanation, enhancement of polyplex uptake was attempted through the addition of cell penetrating and endosomal escape peptides. These peptides (Table 3) are mostly cationic, allowing them to bind directly to the anionic lipids in the cell membrane[69]. Two exceptions are the amphipathic pH-sensitive endosomal escape peptides GALA-CG and INF7, which destabilize the endosomal membrane via the conformational change into pore forming peptides, induced by the acidity of the late endosome[70–72]. The transfection set-up for this peptide screen is similar to the transfection assay as described above, except only HEK 293T and KHYG-1 cells were tested, and both were transfected in serum-free medium with the peptide added in-solution. Serum-free medium was now also applied in NK cells, as it was suggested that serum proteins may competitively engage with cell surface receptors and shield the cationic surface charge of polyplexes, thereby reducing the availability for (receptor-mediated) polyplex uptake[67,73]. Peptide concentrations were based on previous literature[74–79] and consequently increased or decreased upon signs of no transfection or high toxicity, respectively. In HEK 293T cells, the most eGFP positive cells were observed in the positive control with PEI-based polyplexes, which did not improve upon the addition of any peptide (Figure 5A). As PEI transfection rates drop with the addition of all peptides, it was first suggested that the anionic nature of certain peptides (i.e., GALA-CG & INF7) interfere with the electrostatic interaction between mRNA and polymer, causing the polyplex to release its cargo before cellular take-up, similar to the mechanism of heparin-induced release. However, this hypothesis was opposed by the lack of mRNA release on a gel retardation assay (Figure S6C).

*Table 3. Peptides combined with polyplex-transfection in HEK 293T & NK cells.*

| Peptide | Sequence | Charge pH 7 | Charge pH 4.5 | Concentration (µM) | Ref |
|---------|----------|-------------|---------------|--------------------|-----|
| GALA-CG | WEAALAEALAEALAEHLAEALAEALEALAACG | -7 | -3 | 21 | 78,79 |
| INF7 | GLFEAIEGFIENGWEGMIDGWYGC | -5 | -3 | 24 | 76,77 |
| Arg9 | RRRRRRRRR | +9 | +9 | 10 | 80 |
| LAH5 | KKALLALALHHLAHLAHHLALALKKA | +4.5 | +8 | 5, 10, 20, 50 | 74,75 |
| ppTG20 | GLFRALLRLLRSLWRLLLRA | +5 | +5 | 10, 15 | 81 |
| L17E | IWLTALKFLGKHAAKHEAKQQLSKL-amide | +5 | +7 | 10, 15 | 82 |
| CM18-PTD4 | HHHHHHHKWKLFKKIGAVLKVLTTGYARAAARQARA | +8.5 | +14 | 10 | 83 |
| S10 | KWKLARAFARAIKKLGGSGGGSYARALRRQARTG | +10 | +13 | 10 | 84 |

Peptides LAH5 and ppTG20 increased the transfection efficiency in combination with polyplexes from $P_5D_{39}$ and the latter also with pHPMA-DEAE, yet this eGFP expression is not significantly higher compared to the peptide combined with free mRNA. This suggests that the observed transfection is likely not a result from increased polyplex uptake, but rather due to direct complexation of mRNA with the cationic peptides, forming a particle capable of mRNA delivery[74,75,81,83]. Notably, the increase in peptide-associated transfection efficiency is paired with a decrease in viability of the cells, indicating moderate toxicity caused by these peptides at functional concentrations. This is supported by the concentration screening of LAH5 (Figure S6A&B). In KHYG-1 cells, no eGFP positive cells were detected (Figure 5B), showing that the addition of uptake-facilitating or endosomal escape peptides does not improve functional mRNA delivery of these polyplexes.
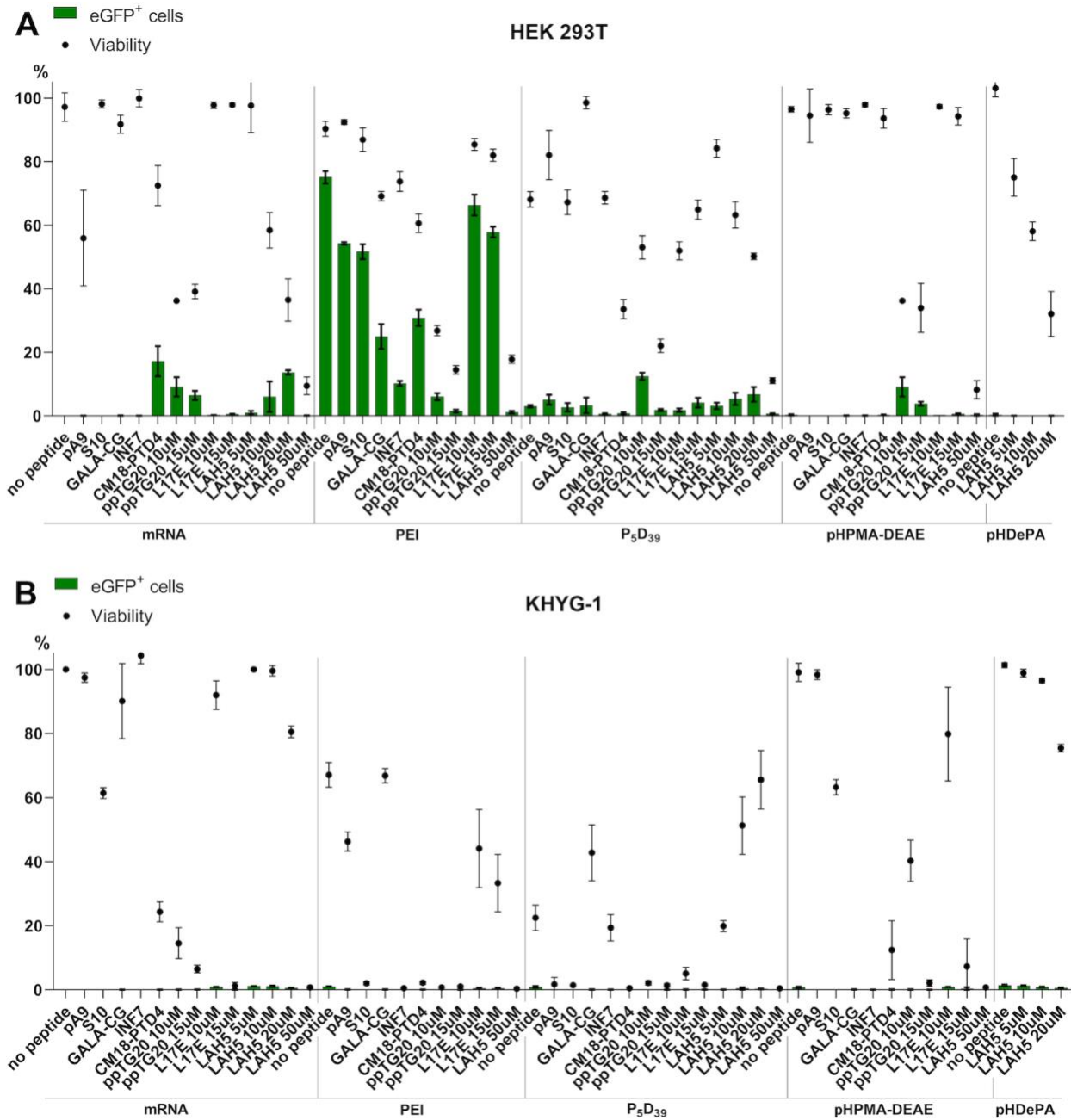
*Figure 5. Peptide-polyplex transfections of (A) HEK 293T and (B) KHYG-1 cells.*

As the additional positive charge from these peptides fails to induce transfection with cationic polyplexes, and simultaneously causes toxicity in HEK 293T and NK cells, the overall use of cationic particles may not be a viable option for NK cell transfection. Hence, an alternative approach must be sought, for instance the adoption of neutral-to-anionic lipid nanoparticles as mRNA delivery system.

# 3. Results & Discussion: Lipid Nanoparticles

## 3.1 Lipid 5 with an N/P Ratio 5 Provides Most Efficient LNP for KHYG-1 Transfection

Preliminary experiments within our research group had shown successful transfection of KHYG-1 cells (50-75% eGFP positive cells) via LNP-mediated delivery of mRNA, with the use of ionizable lipids SM-102 and Lipid 5 (unpublished). As the initial formulation of this LNP was based on literature for *in vivo* transfection[85], the mRNA LNPs were specifically optimized for *ex vivo* NK cell transfection, starting with the optimization of the N/P ratio for each ionizable lipid (Figure 6). As the overall optimization is specific for NK cells, only KHYG-1 cells were tested in these experiments by 24 hour-incubation with low and high dose mRNA-LNPs, in the presence and absence of serum. Low and high dose are defined as 500 ng and 1000 ng of mRNA, respectively, assuming complete mRNA encapsulation and not accounting for any loss during production. The influence of the N/P ratio on zeta-potential of LNPs is clearly illustrated by the characteristics of Lipid 5 LNPs (Table 4); as the N/P ratio increases, the particle surface charge gradually increases from anionic towards a more neutral complex. This reaches its optimum for transfection at N/P 5, where the particle displays a relatively neutral zeta-potential while still showing good tolerability and monodispersity compared to higher N/P ratios. For SM-102, the optimal N/P ratio is 3 (Figure 6A&B), however it should be noted that the SM-102 LNP for N/P 4 was not properly tested as a formulation error has likely caused its overall lack of transfection. This assumption was supported by the great deviation in size and zeta-potential compared to the formulations with N/P ratios 3 and 5 (Table 4). Comparing the ionizable lipids at their optimal N/P ratios, the percentage of eGFP positive cells does not significantly differ between Lipid 5 and SM-102, with both formulations providing high transfection rates of 80-85% eGFP positive cells (Figure 6A). However, analyzing their transfection efficiency by the intensity of the fluorescent signal as a quantification of total eGFP expression (i.e., Mean Fluorescent Intensity; MFI), shows significantly more fluorescence with Lipid 5 LNPs (Figure 6B), thus inducing more efficient transfection than SM-102-based LNPs. In a later stage of optimization, when other components of the LNP formulation had been altered, higher N/P ratios for Lipid 5 were also assessed, yet this led to decreased transfection and viability (Figure 6C&D). Similar to polyplexes, high N/P ratios in LNPs may induce toxicity due to the presence of free ionizable lipids, which become protonated in the acidic endosomal environment[59,60]. Hence, in further experiments, Lipid 5 with an N/P ratio of 5 was used for NK cell transfection. Additionally, the presence of serum resulted in more eGFP positive cells than serum-free conditions (Figure S7A), therefore NK cells incubation with LNPs were further only performed in full medium.

Table 4. mRNA-LNP characterization.

| Ionizable Lipid | N/P ratio | Cholesterol analogue | PEG% | Flow (mL/min) | Volume ratio | Cargo | Size[a] (nm ± SD) | PDI[a] | ζ-potential[b] (mV ± SD) | EE%[c] |
|---|---|---|---|---|---|---|---|---|---|---|
| SM-102 | 3 | Cholesterol | 1.5% | 4 | 1:3 | mRNA | 109 ± 1.9 | 0.08 | -3.69 ± 0.68 | 100% |
| SM-102 | 3 | Cholesterol | 1.5% | 11 | 1:1.5 | mRNA | 102 ± 1.5 | 0.10 | -2.53 ± 0.07 | 100% |
| SM-102 | 3 | Cholesterol | 1.5% | 4 | 1:1.5 | mRNA | 105 ± 2.7 | 0.10 | -3.53 ± 0.83 | 100% |
| SM-102 | 4 | Cholesterol | 1.5% | 4 | 1:1.5 | mRNA | 229 ± 18[d] | 0.37[d] | -16.6 ± 0.74[d] | NT[e] |
| SM-102 | 5 | Cholesterol | 1.5% | 4 | 1:1.5 | mRNA | 109 ± 3.1 | 0.22 | -2.73 ± 0.29 | NT |
| Lipid 5 | 3 | Cholesterol | 1.5% | 4 | 1:1.5 | mRNA | 104 ± 1.5 | 0.24 | -6.20 ± 1.35 | NT |
| Lipid 5 | 4 | Cholesterol | 1.5% | 4 | 1:1.5 | mRNA | 112 ± 0.6 | 0.21 | -5.61 ± 0.74 | NT |
| Lipid 5 | 5 | Cholesterol | 1.5% | 4 | 1:1.5 | mRNA | 110 ± 5.0 | 0.25 | -4.86 ± 1.86 | 76% |
| Lipid 5 | 5 | Cholesterol | 1.5% | 4 | 1:3 | mRNA | 92 ± 1.7 | 0.20 | -3.82 ± 0.26 | 100% |
| Lipid 5 | 5 | Cholesterol | 1.5% | 11 | 1:1.5 | mRNA | 92 ± 17 | 0.49 | -2.31 ± 1.41 | 85% |
| Lipid 5 | 5 | Stigmasterol | 1.5% | 11 | 1:1.5 | mRNA | 82 ± 5.3 | 0.63 | -6.10 ± 1.14 | 60% |
| Lipid 5 | 5 | β-sitosterol | 1.5% | 11 | 1:1.5 | mRNA | 86 ± 13 | 0.48 | -2.55 ± 0.64 | 53% |
| Lipid 5 | 6 | β-sitosterol | 1.5% | 11 | 1:1.5 | mRNA | 100 ± 6.9 | 0.83 | -2.75 ± 1.21 | 43% |
| Lipid 5 | 7 | β-sitosterol | 1.5% | 11 | 1:1.5 | mRNA | 88 ± 8.0 | 0.57 | -3.70 ± 0.44 | 26% |
| Lipid 5 | 5 | β-sitosterol | 2.5% | 11 | 1:1.5 | mRNA | 63 ± 7.3 | 0.63 | -2.94 ± 0.47 | 57% |
| Lipid 5 | 5 | β-sitosterol | 1.5% | 11 | 1:1.5 | pDNA | 159 ± 18 | 0.41 | -2.46 ± 0.27 | NT |
| Lipid 5 | 5 | β-sitosterol | 1.5% | 9 | 1:1.5 | mRNA | 137 ± 6.3 | 0.33 | -2.84 ± 0.20 | 31% |
| **Lipid 5[f]** | **5** | **β-sitosterol** | **1.5%** | **9** | **1:3** | **mRNA** | **133 ± 2.3** | **0.19** | **-1.96 ± 0.54** | **31%** |

[a]Determined by DLS. [b]Determined by Zetasizer. [c]EE% = encapsulation efficiency percentage. [d]Formulation error. [e]NT = not tested. [f]Final optimized LNP formulation.
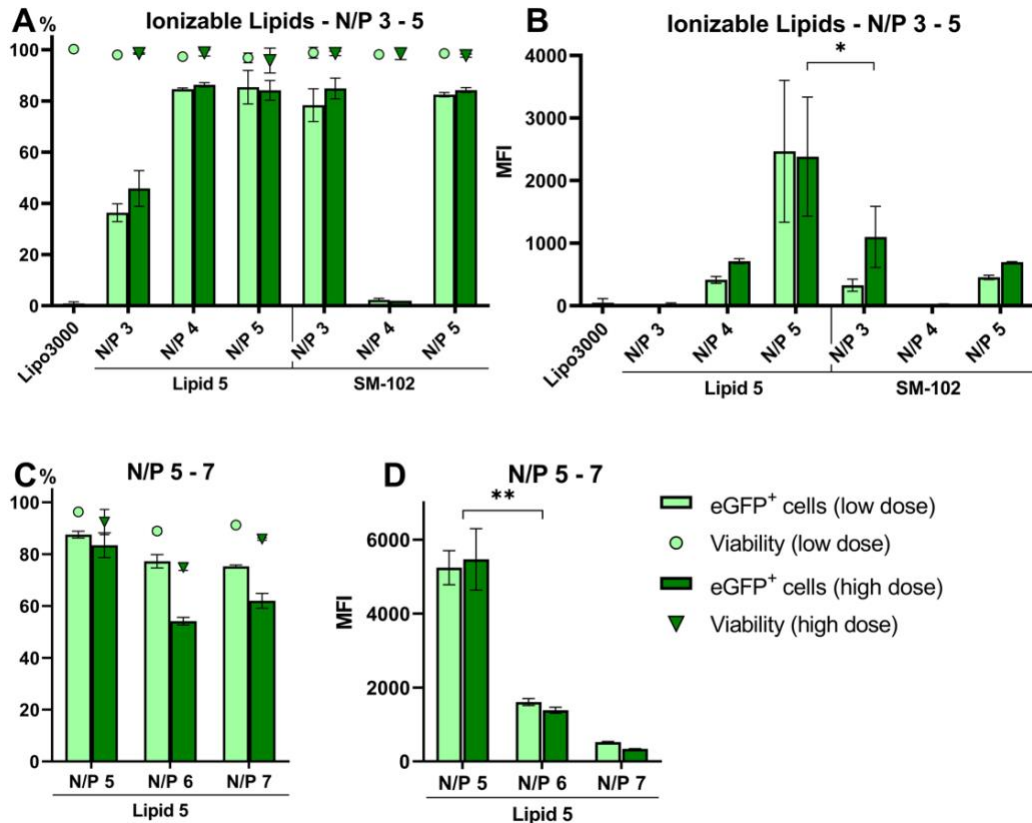


Figure 6. Ionizable lipid & N/P ratio optimization for LNP-based transfection of KHYG-1 cells. (A) Percentage of eGFP positive cells and cell viability, and (B) MFI values for ionizable lipids SM-102 and Lipid 5 at N/P ratios 3 to 5. (C) Percentage of eGFP positive cells and viability, and (D) MFI values for Lipid 5 at N/P ratios 5 to 7. *p<0.05, **p<0.01.

## 3.2 Cholesterol Analogue β-Sitosterol Improves Transfection Efficiency

As for most nucleic acid delivery systems, endosomal escape forms one of the major barriers for functional gene delivery by LNPs[86], yet this barrier can be overcome by the replacement of cholesterol with its plant-based structural analogue β-sitosterol. Not only does the use of β-sitosterol significantly increase the percentage of transfected cells (Figure 7A) but it also greatly enhances the fluorescent intensity and thus total eGFP expression by the NK cell population (Figure 7B). Stigmasterol, another cholesterol analogue, lowers the transfection efficiency, suggesting the specific structure of the analogue is of great importance for its transfection-increasing effect. No significant difference can be observed in zeta-potential and size between the cholesterol and β-sitosterol LNPs (Table 4), therefore the reasoning behind these changes in transfection efficiency must be explained otherwise. A publication by Patel et al. from 2020[87] poses that β-sitosterol maintains the internal structure of the LNP, whilst morphing the originally spherical outer shell to a polyhedral shape. The increased fragility from this structural change induces higher endosomal retention and may promote fusion of the LNP with the endosomal membrane. This allows for a steady subsequent release into the cytosol over time. The increased endosomal retention may also result from less interactions between the LNP and lysosomal transporters, providing the LNP with prolonged residence time to accomplish endosomal escape. Moreover, the altered surface composition possibly promotes different trafficking pathways, which favor endosomal escape[87].
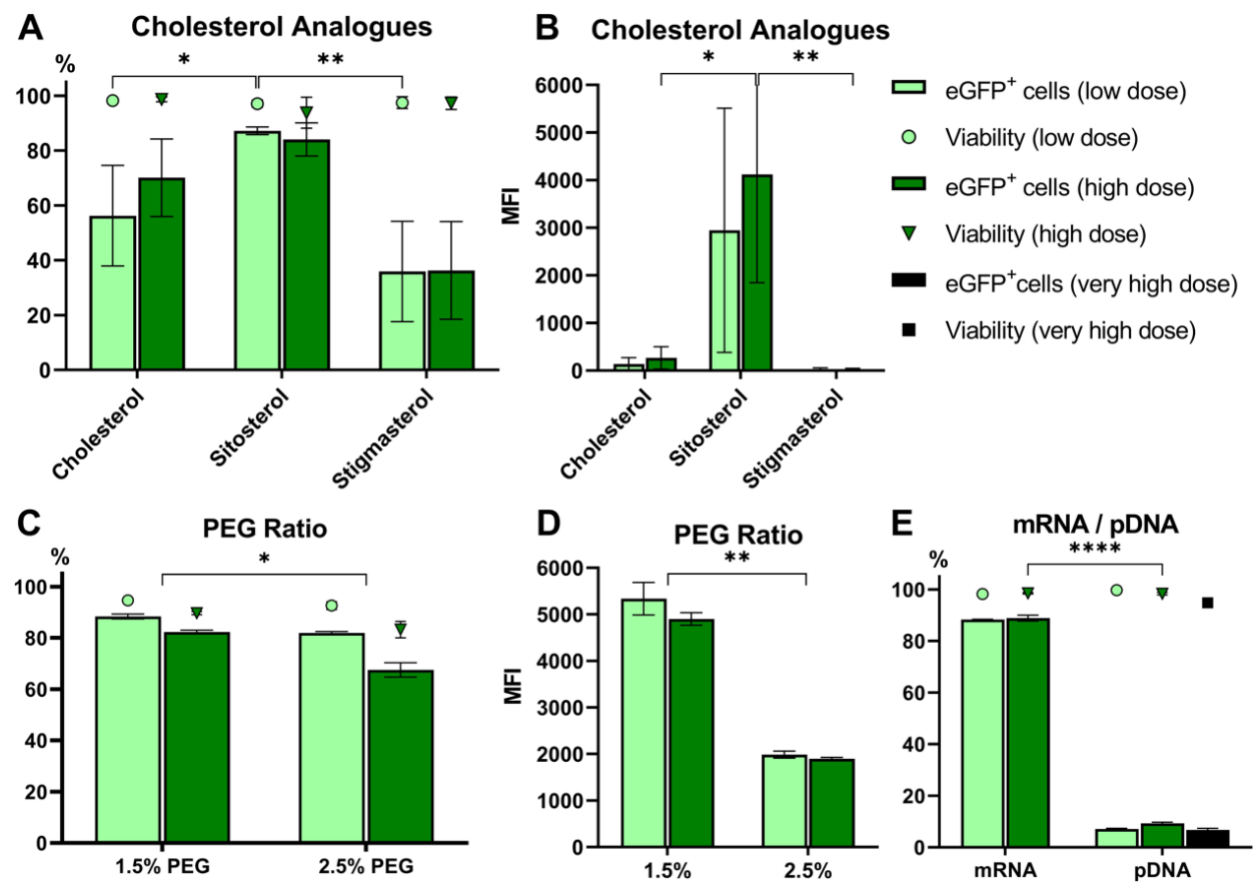


*Figure 7. LNP-formulation optimizations for transfection of KHYG-1 cells. Comparison of cholesterol analogues for their effect on the (**A**) percentage of eGFP positive cells and viability, and (**B**) MFI values. (**C**) Percentage of eGFP positive cells and viability, and (**D**) corresponding MFI values upon an increase in PEG ratio. (**E**) mRNA versus pDNA LNP cargo presented as percentage of eGFP positive cells and viability. \*p<0.05, \*\*p<0.01, \*\*\*\*p<0.0001.*

## 3.3 LNP Size Reduction (by Increased PEG content) Does Not Enhance NK Transfection

The size of nanoparticles is of significant importance for its gene delivery functionality as the pathway of cellular uptake (and subsequent endosomal encapsulation) is highly dependent on size. Herein, smaller particles are generally associated with higher transfection efficiency[56,88]. Reducing particle size, whilst maintaining a consistent N/P ratio, can be achieved by increasing the PEG ratio in the lipid composition[56,89], which was confirmed for our LNP formulation when the size reduced from 86 to 63 nm upon a PEG increase from 1.5% to 2.5% (Table 4). However, the smaller LNP induced significantly lower transfection rates, both in percentage of eGFP positive KHYG-1 cells and total fluorescent signal (Figure 7C&D). Besides decreasing size, increasing PEG content also stabilizes LNPs through formation of an outer hydrophilic shell, thus possibly reducing cellular uptake[89], endosomal escape[90] and cargo release[89], which could explain the decrease in transfection efficiency. Lower cellular uptake may also result from reduced protein-lipid interactions by PEGs shielding properties[90].

## 3.4 mRNA versus pDNA Cargo for LNP Formulation

As shown by previous experiments, the formulated nanoparticle can achieve functional delivery of genetic material in the form of mRNA. To verify whether transfection was reliant upon mRNA delivery (rather than general nucleic acid delivery), our current LNP formulation was prepared with eGFP-encoding plasmid DNA (pDNA) instead of mRNA. This preparation led to a great increase in particle size (from ~85 to ~160 nm) (Table 4), and subsequently a significant drop in transfection of KHYG-1 cells (Figure 7E). Besides the altered LNP properties, the lack of reported transfection also may result from cytosolic cargo delivery, as this does not allow for transcription of the pDNA and hence no translation of the genetic code into a fluorescent signal. However, it should be noted that the 24-hour incubation period is likely too brief to observe DNA-based transfections, since pDNA transport to the nucleus and transcription initiation are extra time-consuming steps. Hence, these results merely suggest that the current formulation and experimental set-up were solely optimized for mRNA delivery, and further conclusions on cargo specificity require additional transfection assays with prolonged incubation time.

## 3.5 Microfluidics Optimization on NanoAssemblr®

Synthesis of LNPs is based on combining a lipids mixture in ethanol with the nucleic acid cargo in aqueous acidic buffer, in a chaotic mixing system. This results in the formation of LNPs in an acidic-buffered ethanol solution, which is subsequently dialyzed against a physiological buffer to obtain neutral particles without residual ethanol. To provide an easily scalable production method of the LNPs, we used the NanoAssemblr® microfluidics device, which allows for a variability in flow and volume ratio during lipid and mRNA mixing. As these device-specific parameters considerably influence particle size and PDI[58,91,92], they were optimized on multiple occasions throughout the LNP optimization process. A preliminary flow rate and volume ratio screening with cholesterol-based LNPs showed highest transfection efficiency (based on MFI) at a high flow rate of 11 mL/min, with a lipid-to-mRNA ratio of 1:1.5 (Figure S7B&C). Although the LNP became smaller and more polydisperse upon this change in flow rate (Table 4), the transfection efficiency was not influenced by the polydisperse mixture, hence the high flow rate and 1:1.5 volume ratio were also applied as the LNP formulation switched from cholesterol to the β-sitosterol analogue. After performing the above-described optimization assays, these NanoAssemblr® parameters were reassessed for the new particle formulation; this was partially initiated because the LNPs seemed to completely lose their transfection efficiency after several batch preparations (Figure S7D). It remained unclear as to why this sudden transfection decrease occurred, but suspected is a lack of LNP stability due

to β-sitosterol incorporation, as visible aggregation started to form after microfluidic mixing of the high flow-1:1.5 volume ratio formulation. By slowing the flow rate to 9 mL/min and changing the lipid:mRNA ratio to 1:3, as is reported in literature[85], no visible LNP aggregates could be observed, transfection efficiency was restored, and total eGFP expression significantly increased (Figure 8A&B). For the sake of proper comparison, only the first four functional batches of β-sitosterol-based LNPs (prepared with flow 11 mL/min & 1:1.5 volume ratio) were included in Figure 8A&B. The stability increase following the volume ratio change is likely resulting from a higher acidic buffer (and lower ethanol) percentage during microfluidics, which allows for more protonation of the ionizable lipid, and thus stronger complexation with the mRNA. Moreover, the ethanol percentage and flow rate are known to affect LNP size and PDI[58], where the preferred volume ratio of 1:3 and 9 mL/min flow rate correspond to more monodisperse particles (Table 4). In the last stage of NanoAssemblr®-specific microfluidics optimization, the two parameters were assessed in umbilical cord blood derived-primary NK cells, which supported the previously optimized settings of 9 mL/min and a 1:3 lipid:mRNA ratio by presenting 75% eGFP positive cells (Figure 8C&D).
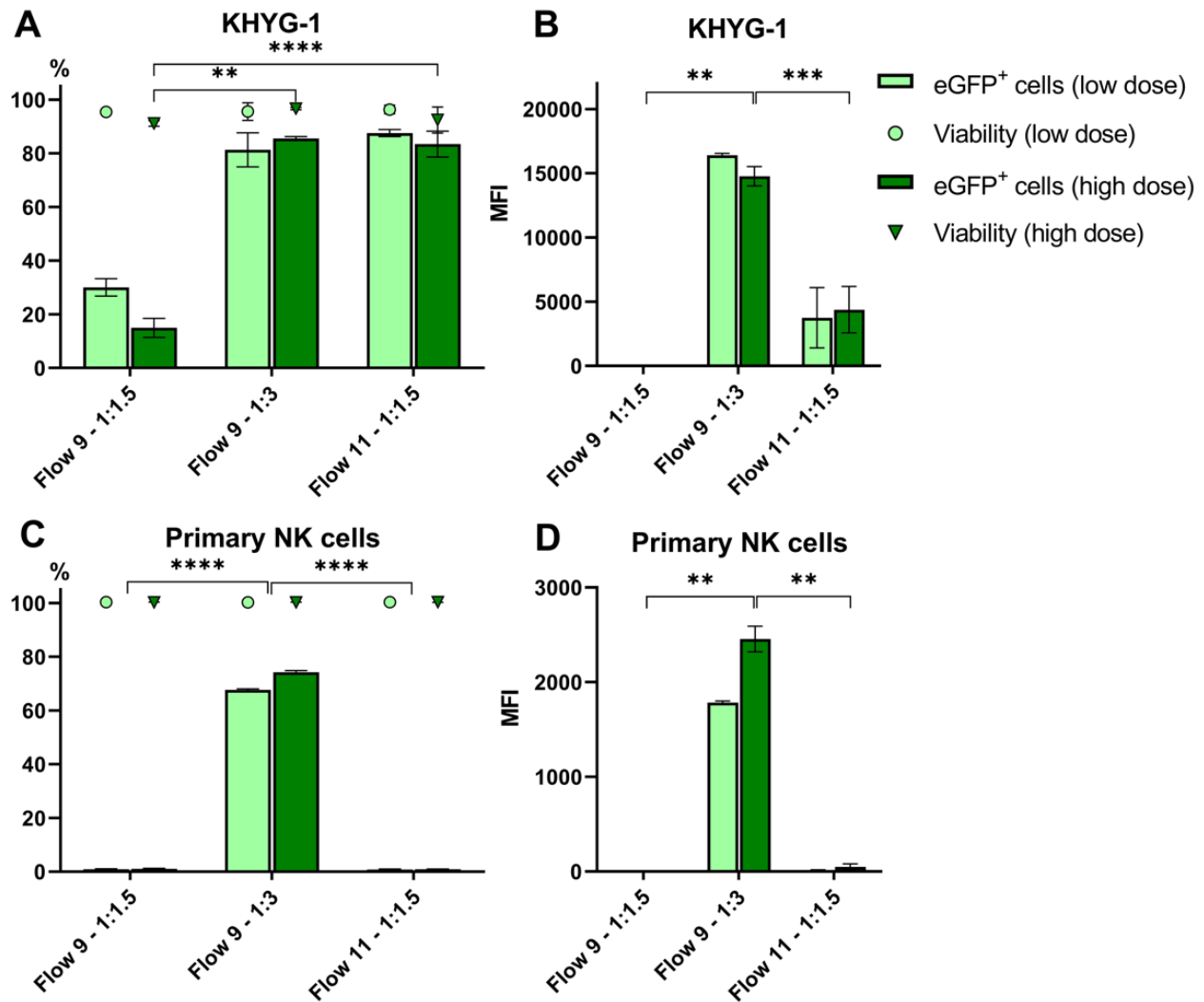


*Figure 8. Microfluidics LNP optimizations in KHYG-1 and primary NK cells. NanoAssemblr® settings comparison for KHYG-1 presented as (**A**) eGFP positive cells and viability, and (**B**) total fluorescent signal (MFI), showing the same optimal formulation for cord blood-derived primary NK cells (**C&D**, respectively). \*\*p<0.01, \*\*\*p<0.001, \*\*\*\*p<0.0001.*

## 3.6 (Primary) NK Cell Transfection with mRNA-LNPs is More Efficient Than Electroporation

Ultimately, the optimized mRNA-LNP formulation was compared to the currently most effective nonviral transfection method of NK cells, electroporation[7,42]. In KHYG-1, the rate of transfection was significantly higher for LNP-based transfection than electroporation, at 85% versus 76% of eGFP positive cells, respectively (Figure 9A). The difference between these methods becomes even more notable when comparing their fluorescence as a measure of total eGFP expression: transfection with LNPs presents a 16-fold increase in MFI over electroporation of KHYG-1 cells (Figure 9B). Encouraged by these results, the LNP-versus-electroporation comparison was carried out in cord blood-derived primary NK cells; this showed successful primary NK cell transfection with our mRNA-LNP formulation, with transfection rates at ~75% eGFP positive cells (Figure 9D). This is significantly higher than the observed 57% transfection rate in electroporated primary cells, proving that our LNP-based transfection method is not only performing better in NK cell lines, but also in clinically relevant NK cells. Once again, these positive outcomes are supported by the MFI, reporting a 5.5-fold increase between high-dose LNPs and electroporation (Figure 9E). The rise in LNP-induced fluorescence is clearly visualized by confocal live cell imaging of both KHYG-1 and primary NK cells (Figure 9C&F), demonstrating that the intracellular eGFP expression is indeed more pronounced in LNP-transfected cells compared to electroporated ones. Thus, transfection with LNPs seems more efficient than electroporation. Supposedly, this is the result of longer mRNA exposure as cells are continuously incubated in the presence of LNPs, providing 24 hours to allow mRNA uptake and subsequent translation. Alternatively, electroporation serves a pulse of merely 50 μs in which mRNA can be delivered into the cell. Moreover, the harsh conditions of this pulse may introduce (non-lethal) damage to both cells and mRNA. In electroporated cells, metabolic stress as a result of cation influx has been reported, leading to suppression of protein synthesis and hence reduced mRNA expression[93–95]. As for mRNA damage, multivalent cations are released from the metal cuvettes during electric pulsing, which can subsequently co-precipitate with the mRNA, hence consuming part of the genetic material[96,97]. Besides causing aggregation, these metal ions may also induce cleavage of ribonucleotides[97,98], thus further reducing the mRNA available for transfection.
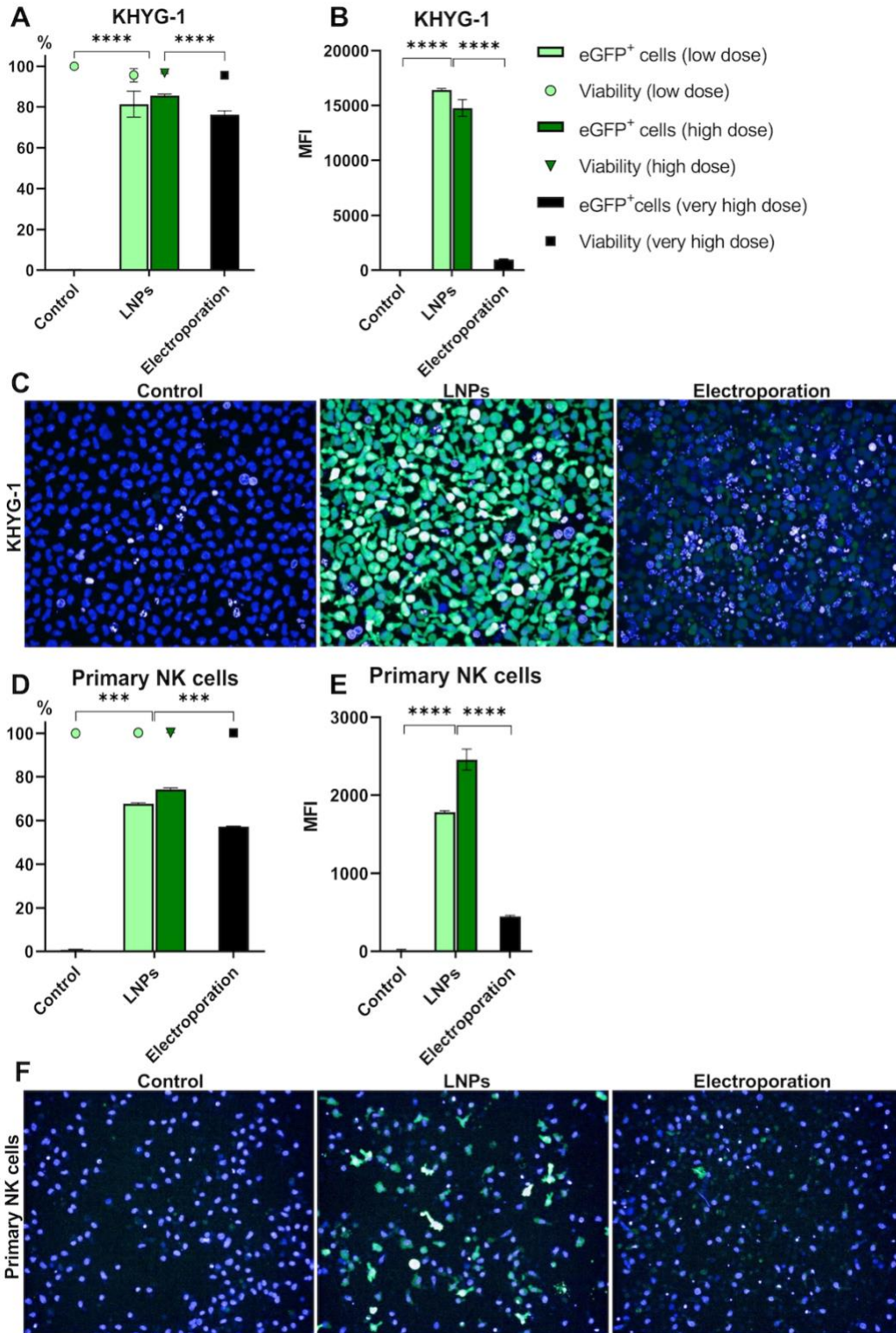
*Figure 9. Comparison of LNP-based transfection and electroporation in KHYG-1 cells and cord blood-derived primary NK cells. (**A**) Percentage of eGFP positive KHYG-1 cells and (**B**) their corresponding MFI values, analyzed by FACS. (**C**) Visualization of transfection efficiency in KHYG-1 cells via confocal live cell imaging; green fluorescence indicates eGFP expression while cell nuclei are stained blue with Hoechst. For cord blood-derived primary NK cells, identical parameters are presented in figures **D**, **E** and **F**, respectively. \*\*\*p<0.001, \*\*\*\*p<0.0001.*

# 4. Conclusion & Future Prospects

To summarize, cationic mRNA-polyplexes prepared with pHPMA-DEAE, pDePA, PUBAP, $P_5D_{39}$ or PEI were successfully synthesized, yet none were able to transfect NK cells. The addition of peptides during polyplex incubation, which should aid in enhancing cellular uptake and endosomal escape, did not improve the lack of transfection efficiency, but contrarily mostly caused cytotoxicity. On the other hand, mRNA-loaded LNPs resulted in transfection efficiency up to ~85% in the NK cell line KHYG-1. Optimization of the initial formulation, by employing an N/P ratio of 5 with Lipid 5 as ionizable lipid, using β-sitosterol instead of cholesterol as steroid, and applying a 1:3 lipid:mRNA ratio with a flow rate of 9 mL/min during microfluidics, resulted in a significant increase of transfection efficiency and in the overall fluorescent signal of eGFP. Not only is the optimized LNP formulation able to transfect the clinically relevant umbilical cord blood-derived primary NK cells, but it also significantly outperforms the currently most used nonviral method of (primary) NK cell transfection, electroporation. Observing the success of LNPs compared to polyplexes, it can be hypothesized that a negative-to-near-neutral particle may be more suited for NK cell transfection than highly cationic particles. The lack of transfection upon addition of cationic peptides supports this hypothesis. Preliminary uptake studies with the prepared polyplexes (data not discussed in this report) suggest that the highly charged particles are not taken up by NK cells, which is significantly improved when using near-neutral LNPs. Moreover, a destabilized nanoparticle structure, obtained by replacing cholesterol with β-sitosterol, results in higher transfection, suggesting that a "too stable" particle may not allow cellular uptake, endosomal escape, or sufficient mRNA release. To further elucidate this hypothesis, LNP imaging with electron microscopy may provide useful insights in the difference between particle structure of cholesterol- and β-sitosterol-based LNPs; the suggested polyhedral shape with β-sitosterol could thus be confirmed. As a more fragile LNP is expected with this change in steroid, stability studies must be performed to assess the robustness of the optimized formulation. This can also prove useful in case of later clinical applications. Regarding clinical applications, it would be relevant to filter the prepared LNPs through 0.2 μm sterilization filters, as some form of sterilization would be required for regulatory approval.

However, before any type of clinical application can be considered, the LNPs must be tested with biologically relevant cargo. Towards this end, mRNA can be used that encodes activating (i.e., CD16, NKp30, NKp44, NKp46, NKG2C and NKG2D) or chemokine receptors (i.e., CXCR3–CXCR4, CX3CR1 and CCR3–CCR5), which would allow for (over)expression of the respective protein, ultimately enhancing anti-tumor activity of the transfected NK cell. When performing this research, the increase in receptor expression should not only be measured, but also the durability of this expression. Although we employ 5-methoxyuridine-modified mRNA for increased nucleic acid stability and reduced immunogenicity[99], mRNA still degrades in the cytosol over time and thus is protein expression expected to be of short duration compared to viral methods that allow for transient expression[44,85]. This could be considered as the main limitation of LNP-based NK cell transfection; multiple LNP transfections may be required to generate a sufficient phenotypical change for clinical application. To this end, experiments with longer incubation times (>72 hours) in the absence and presence of LNPs have to be done to assess the durability of protein expression. Linear or plasmid DNA may also be adopted as LNP cargo, if proven effective in future experiments, to allow for more sustained protein expression; mRNA was preferred as a starting point for this research since it only requires cytosolic delivery and thus circumvents the need for cargo transport to the nucleus.

Finally, NK cells may be generated with multiple (over)expressed receptors via the delivery of various mRNA templates, encapsulated within the same LNP. This would be a major advantage compared to requiring multiple rounds of electroporation for efficient transfection with multiple genes. Related to electroporation, a phenotypical comparison between electroporated cells and LNP-transfected cells can be researched to exclude the possibility of LNPs causing a similar change in NK phenotype as observed for electroporation[44].

By transfecting primary NK cells with mRNA-LNPs encoding for receptors that promote anti-tumor activity, NK cells are becoming one step closer to their application for adoptive cell therapy, and hence a novel approach for fighting therapy-resistant cancer.

# 5. Materials & Methods

## 5.1 Materials

Carbonic acid 2-diethylamino-ethyl ester 1-methyl-2-(2-methacryloylamino)-ethyl ester (HPMA-DEAE) was synthesized as reported by Luten et al[52]. N-[2-(2-pyridyldithio)]ethyl methacrylamide (PDTEMA) and 2-azidoethylmethyacryl-amide (AzEMAm) were synthesized as reported by Bo Lou et al[51]. The block copolymer $P_5D_{39}$, consisting of a 5 kDa poly(ethylene glycol) (PEG) block covalently linked to a 39 kDa poly(2-(dimethylamino)ethyl methacrylate) (PDMAEMA) block was a gift from Cristina Casadidio (Utrecht University, the Netherlands). Linear polyethyleneimine (PEI, Mw 25 kDa) was obtained from Polysciences (Warrington, USA). Ionizable lipid 8-[(2-hydroxyethyl)[6-oxo-6-(undecyloxy)hexyl]amino]-octanoic acid, 1-octylnonyl ester (SM-102) was obtained from DC Chemicals (Shanghai, China) and ionizable lipid 8-[(2-hydroxyethyl)[8-(nonyloxy)-8-oxooctyl]amino]-octanoic acid, 1-octylnonyl ester (Lipid 5) was obtained from Cayman Chemical (Ann Arbor, USA). Helper lipid stigmasterol was purchased from Avanti Polar Lipids (Alabama, USA) and 1,2-distearoyl-sn-glycero-3-phosphocholine (DSPC) was purchased from Lipoid (Ludwigshafen, Germany). 1,2-Dimyristoyl-sn-glycero-3-methoxypolyethylene Glycol (DMG-2kPEG), was purchased from NOF (Frankfurt am Main, Germany). Unpurified side chain-protected GALA-CG peptide on Wang-resin was provided by Antoinette van den Dikkenberg (Utrecht University, the Netherlands). All other peptides were purchased at >99% purity from Synpeptide Co (Shanghai, China). Enhanced Green Fluorescent Protein (eGFP) encoding mRNA with 5-methoxyuridine was obtained from Tebu-bio (TriLink, San Diego, USA). Plasmid DNA (pDNA) encoding eGFP was provided by Olivier de Jong (Utrecht University, the Netherlands). Lipofectamine[TM] 3000, Lipofectamine[TM] LTX, non-sterile phosphate buffered saline (PBS), Slide-A-lyzer® Dialysis cassettes (Extra Strength) (Molecular weight cut-off, MWCO: 10 kDa), Qubit™ RNA BR Assay Kit & Quant-iT™ RiboGreen™ RNA Assay Kit, and Hoescht 33342 were purchased from Thermo Fisher Scientific (Bleiswijk, the Netherlands). For KHYG-1 cell culture, RPMI 1640 medium with L-glutamine was obtained from Capricorn Scientific (RPMI-A, Ebsdorfergrund, Germany). For NK-92 cells, BioWhittaker® Alpha MEM with (desoxy)ribonucleotides and UltraGlutamine 1 was purchased from Lonza (Verviers, Belgium). Recombinant human interleukin-2 with "Improved Sequence" was obtained from Miltenyi Biotec (Bergisch Gladbach, Germany). For flow cytometry analysis, either Zombie NIR[TM] from BioLegend (Uithoorn, The Netherlands) or 7-Aminoactinomycin D (7-AAD) from Sigma-Aldrich (Schnelldorf, Germany) was used as viability stain. APC-Alexa Fluor* 750-conjugated anti-human CD56 antibody (CD56-APC-A750, N901) and Krome Orange-conjugated anti-human CD45 antibody (CD45-KrO, J33) were obtained from Beckman Coulter Lifesciences (Woerden, The Netherlands). All solvents were obtained from Biosolve (Valkenswaard, the Netherlands), and dried for at least 24 hours by activated molecular sieves (4A) when used during polymer synthesis. DMEM medium and all other chemicals and reagents were purchased from Sigma-Aldrich (Zwijndrecht, the Netherlands) and used as received.

## 5.2 Polymer Synthesis & Peptide Purification

### 5.2.1 pHDePA

Triblock co-polymer poly(HPMA-DEAE-*co*-PDTEMA-*co*-AzEMAm) (pHDePA) was synthesized similar to the previously reported pHDPA[51]. pHDePA was synthesized by free radical polymerization under nitrogen atmosphere with a monomer to initiator ratio (M/I) of 20. The molar feed ratio of monomers was 70/20/10 for HPMA-DEAE, PDTEMA and AzEMAm, respectively. In a flask sealed with rubber septum, 220 mg HPMA-DEAE (0.77 mmol), 56.7 mg PDTEMA (0.22 mmol), 17 mg AzEMAm (0.11 mmol), and 6 mg azobisisobutyronitrile (AIBN, 0.02 mmol) were dissolved in dry DMSO (1 mL) and subjected to three vacuum-$N_2$ cycles. Polymerization was continued at 70 °C for 24 hours under constant nitrogen flow. The resulting orange mixture was diluted with DMF (2 mL), after which the polymer was precipitated in cold

diethyl ether. The polymer was redissolved in DMF and precipitated again to a total of 3 times. After extensive dialysis (8 kDa MWCO) against 10 mM ammonium acetate ($NH_4OAc$) buffer at pH 5 for 3 days, pHDePA was retrieved as a white fluffy powder upon freeze drying. Molecular weights and polydispersity (PDI) were determined by Gel Permeation Chromatography (GPC) as described below. The monomer ratio was determined by ^{1}H-NMR in DMSO-$d_6$ through comparison of the integrals at δ 4.71 ppm (bs, O$CH_2$CH₂, 2H, HPMA-DEAE), δ 7.2-7.8 ppm (m, pyridyl proton group, 4H, PDTEMA), and δ 3.65 ppm (m, $CH_2CH_2$N₃, 4H, AzEMAm) (Figure S2).

### 5.2.2 pHPMA-DEAE

Poly(Carbonic acid 2-diethylamino-ethyl ester 1-methyl-2-(2-methacryloylamino)-ethyl ester) (pHPMA-DEAE) was synthesized similar as previously reported by Luten et al[52], by free radical polymerization under nitrogen atmosphere with a M/I ratio of 400. In a flask sealed with rubber septum, 916 mg HPMA-DEAE (3.2 mmol) and 1.3 mg AIBN (0.008 mmol) were dissolved in dry DMSO (1 mL) and subjected to three vacuum-$N_2$ cycles. Polymerization was continued at 70 °C for 20 hours under constant nitrogen flow. The orange reaction mixture was diluted with 10 mM $NH_4OAc$ buffer (pH 5) and extensively dialyzed (3 kDa MWCO) against the same buffer for 3 days. Next, pHPMA-DEAE was freeze-dried and obtained as a fluffy white powder. ^{1}H-NMR (CDCl₃): δ = 6.3 ppm (1H, OC$NH$CH₂), 4.7 ppm (1H, NHCH₂$CH$CH₃), 4.2 ppm (2H, OC=OO$CH_2$CH₂N), 3.4-2.9 ppm (2H, OCNH$CH_2$), 2.7 ppm (2H, OC=OOCH₂$CH_2$N), 2.6 ppm (3H, NHCH₂CH$CH_3$), 1.9 ppm (2H, CH₃C$CH_2$CCH₃ ), 1.2 ppm (4H, 2 x N$CH_2$CH₃), 1.0 ppm (6H, 2 x NCH₂$CH_3$) (Figure S1).

### 5.2.3 PUBAP

The 1,4-bis(3-amino propyl)piperazine (BAP) residue-containing polyurethane (PUBAP) was prepared similarly as reported by Cheng et al[61], via a two-step synthesis.

In the first step, the OH groups on 2,2'-dithiodiethanol (DTDE) were substituted by an esterification reaction with bis(pentafluorophenyl) carbonate (bis5F), to yield 2,2'disulfanediylbis(ethane-2,1-diyl) bis(pentafluorophenyl) bis(carbonate) (DTDE-bis5F) (Scheme S4). In a round bottomed flask, 498 mg DTDE (3.23 mmol), 5.09 g bis5F (12.9 mmol) and 1.67 g DIPEA (12.9 mmol) were combined in dry DCM (20 mL) and left to stir overnight under nitrogen protection at room temperature (RT). The reaction mixture was washed twice with saturated $NaHCO_3$, twice with 0.1 N HCl, once with brine and then dried over $Na_2SO_4$. The DCM was evaporated under reduced pressure, providing an orange oil that was purified by gradient silica column chromatography (9:1 to 1:4 hexane:ethyl acetate) to yield DTDE-bis5F as a pale yellow oil (1.87 g, 100% yield).

^{1}H-NMR (CDCl₃): δ = 4.60 ppm (t, 2 x SS$CH_2$CH₂, 4H), 3.08 ppm (t, 2 x SS$CH_2$CH₂, 4H) (Figure S5).

Secondly, PUBAP was synthesized by polycondensation of DTDE-bis5F and BAP for 3 days. Equal molar parts of DTDE-bis5F (919 mg, 1.60 mmol) and BAP (320 mg, 1.60 mmol) were dissolved in dry DMF and stirred together in the dark at RT under nitrogen. After 24 hours, the reaction was proceeded at 40 °C for 2 more days. The resulting yellow reaction was diluted with Milli-Q water and glacial acetic acid was added until the mixture reached pH 4-5. After extensive dialysis (1 kDa MWCO) against Milli-Q water for 3 days and subsequent freeze-drying, PUBAP was obtained as a white powder (121 mg, 10% yield).

^{1}H-NMR (CDCl₃): δ = 6.09 ppm (2 x OCON$H$CH₂, 2H), 4.30 ppm (2 x SS$CH_2$CH₂, 4H), 3.25 ppm (2 x OCONH$CH_2$, 4H), 2.93 ppm (2 x SS$CH_2$CH₂, 4H), 2.75-2.45 ppm ($CH_2$N$CH_2CH_2CH_2CH_2$N$CH_2$, 12H), 1.25 ppm (CH₂$CH_2$CH₂, 2H), 0.83 ppm (CH₂$CH_2$CH₂, 2H) (Figure S3).

### 5.2.4 GALA-CG

The GALA-CG peptide was synthesized by Antoinette van den Dikkenberg (Utrecht University, the Netherlands) on glycine-preloaded Wang resin with standard Fmoc solid-phase chemistry, including final Fmoc deprotection, using a Liberty blue peptide synthesizer (CEM Corporation). Peptide-containing resin was washed three times with DMF:DCM (50:50) and three times with DCM. Side chain deprotection and cleavage of the peptide from resin was attained by stirring the GALA-CG-resin in a solution of trifluoro acetic acid, triisopropylsilane and Milli-Q (95:2.5:2.5) for 1 hour and RT. Following cleavage, the peptide was precipitated in cold diethyl ether, washed 3 more times with diethyl ether and obtained as a pale yellow pellet after drying. Final purification was performed by means of preparative reversed-phase chromatography on an Alliance 2695 (Waters, the Netherlands) chromatography system equipped with a C18-AQ column (ReproSil-Pur 120, 10 µm, 25 mm X 250 mm) at RT and UV detection (210 nm and 280 nm). The gradient ran with a flow of 5 mL/min starting with Solvent A (10 mm ammonium bicarbonate ($NH_4HCO_3$), 5% ACN in Milli-Q water) to Solvent B (10 mm $NH_4HCO_3$ in ACN) within a timeframe of 50 min, running a total time of 1 hour. Fractions were manually collected upon UV detection above 0.05 AU. Fractions were analysed for GALA-CG presence by reverse-phase HPLC and two types of mass spectrometry (MS); normal resolution electrospray ionization (ESI)-MS measurements were performed on a microTOF-Q II (Bruker), while matrix assisted laser desorption ionization (MALDI)-MS analyses were performed on a Ultraflextreme (Bruker), employing α-cyano-4-hydroxycinnamic acid as the matrix. Fractions solely containing GALA-CG were pooled and freeze-dried to yield the peptide as a white fluffy powder.

## 5.3 Polyplex & LNP Preparation

### 5.3.1 Polyplexes

Polymer stock solutions were prepared in 20 mM HEPES buffer (pH 7.4) at 1 mg/mL (PUBAP), 5 mg/mL ($P_5D_{39}$ & PEI) or 10 mg/mL (pHDePA & pHPMA-DEAE). The commercial 5-methoxyuridine modified eGFP-mRNA is provided at 1 mg/mL in 1 mM sodium citrate (pH 6.4). For polyplex preparation, the calculated amount of stock solutions (based on N/P ratio and amount of required mRNA) were diluted with 20 mM HEPES buffer (pH 7.4) to a total volume of 100 µL for each solution. Then, the polymer solution was added to the mRNA solution in a 1:1 volume ratio (thus resulting in a 200 µL total volume), followed by immediate mixing through manual pipetting. The formed polyplexes were incubated on ice for 15 mins before further use.

### 5.3.2 Lipid Nanoparticles (LNPs)

Lipid nanoparticles (LNPs) were prepared through microfluidic mixing of lipids in organic solvent and mRNA in acidic buffer, similar to previously reported[85]. Briefly, lipids were dissolved in ethanol at molar ratios of 50:10:38.5:1.5 (ionizable lipid:DSPC:cholesterol:DMG-2kPEG) unless otherwise specified. Sodium acetate (NaOAc) buffer at 6.25 mM (pH 5.0) was used to dilute 5-methoxyuridine modified eGFP-mRNA. The lipid mixture and mRNA solution were combined using a NanoAssemblr® microfluidic mixer (Precision Nanosystems, Vancouver, Canada) at a volumetric ratio of 1:1.5 or 1:3 (ethanol:aqueous) with the total flow rate ranging between 4 and 11 mL/min. The obtained LNPs were dialyzed against 1X PBS (pH 7.4) in Slide-A-lyzer® Dialysis cassettes (Extra Strength) (10 kDa MWCO) for at least 12 hours. LNPs were then extracted from the cassettes and stored for a maximum of 24 hours at 4 °C until use.

## 5.4 Cell Transfection Studies

### 5.4.1 Cell Culturing

Human embryonic kidney (HEK 293T) cells, and both NK cell lines (NK-92 and KHYG-1) were obtained from the American Type Culture Collection (ATCC, Manassas, Virginia, USA). HEK 293T cells were cultured in Dulbecco's Modified Eagle Medium (DMEM) supplemented with 10% of fetal bovine serum (FBS), and passaged 3 times a week. KHYG-1 cells were cultured in Roswell Park Memorial Institute (RPMI) 1640 medium/glutamine with 10% FBS and 160 U/mL recombinant human interleukin 2 (IL-2), at a density of 0.3-1x10$^6$ cells/mL by passaging twice a week. NK-92 cells were maintained in Minimum Essential Medium α (alpha-MEM) with L-glutamine and with ribonucleosides, supplemented with 12.5% horse serum, 12.5% FBS and 500 U/mL IL-2. NK-92 cells were passaged 2-3 times a week and cultured at ~0.5x10$^6$ cells/mL after passaging. Primary CD34$^+$ NK cells were generated from cryopreserved umbilical cord blood hematopoietic stem cells by Glycostem Therapeutics (Oss, The Netherlands) and delivered to us together with fully supplemented medium. Upon delivery, deeply frozen CD34$^+$CD45$^+$ cells were thawed (day 1) at 2x10$^6$ cells/mL in Glycostem Basal Growth Medium (GBGM) with 2% horse serum and differentiation cytokine cocktail, consisting of 20 ng/ml of IL-7, SCF, IL-15, and 1,000 U/ml IL-2. This culture was refreshed every 2–3 days and maintained for 7 days, until cell seeding for the transfection assay. All cell lines were cultured at 37 °C in a humidified atmosphere containing 5% of $CO_2$.

### 5.4.2 Transfection Assays

All polyplex- and LNP-based transfection studies were performed in 96-well plates, with cells seeded 24 hours prior to transfection. For initial polyplex studies, 40.000 cells/well were seeded, which was lowered to 25.000 cells/well during peptide-polyplex combination studies; this amount was equal for HEK 293T and NK cell lines. For all LNP-based transfections, 25.000 KHYG-1 cells/well and 18.000 primary NK cells/well were seeded 24 hours prior to LNP exposure. At the day of transfection, cell medium was maintained from the day before or replaced with serum-free medium, as described in the Results & Discussion sections. For polyplex assays, polyplexes were prepared directly before addition to the cells, as described above, and subsequently added at an mRNA concentration of 250 ng/well. Alternatively, LNPs were freshly prepared as described above and administered to the cells right after removal from dialysis cassettes, at a concentration of 500 ng (low dose) or 1000 ng (high dose) of mRNA/well, assuming complete mRNA encapsulation and not accounting for any loss during production. Following particle addition, cells were incubated for 24 hours at 37 °C with 5% of $CO_2$. After incubation, the percentage of eGFP positive cells was quantified by flow cytometry (FACS) and visualized by confocal live cell imaging. In all assays, cells treated with only medium (in the absence or presence of serum depending on transfection experiment) were used as negative control and each condition was measured in triplicate (for polyplexes) or duplicate (for LNPs). Commercially available transfection agents, Lipofectamine™ 3000 and Lipofectamine™ LTX, were prepared according to manufacturer's protocol and added at 150 ng mRNA/well.

### 5.4.3 Electroporation

On the day of transfection, 2x10$^6$ cells per transfection were harvested by centrifugation and subsequently resuspended in 1 mL 0.01% DMSO in OPTI-MEM. Next, cells were pelleted, resuspended in 200 μL 0.1% DMSO in OPTI-MEM and subsequently transported to a 4 mm BTX aluminum cuvette (Holliston, US) for electroporation with 20 μg mRNA/mL at 1 pulse of 1450 V for 50 μs, using a BTX ECM 830 square wave electroporation system (Holliston, US). Cells were then immediately transferred to a prewarmed 6-well plate containing 2 mL of complete medium and incubated for 24 hours at 37 °C with 5% of $CO_2$.

### 5.4.4 Flow Cytometry (FACS)

To quantify transfection with eGFP mRNA and simultaneously assess cytotoxicity of the applied transfection method, flow cytometry (FACS) was performed. For immortal cell lines (HEK 293T, NK-92 & KHYG-1), cells were incubated in the dark at RT for 20-40 min with Zombie NIR™ viability stain (diluted 1:1000 according to manufacturer's instructions) after a wash with 1X PBS. Cells were consequently washed with FACS buffer (1X PBS with 0.5% bovine serum albumin) and fixed in 1% paraformaldehyde (PFA) before analysis by high-throughput screening with a BD FACSCanto™ II Flow Cytometry System (Franklin Lakes, USA). Viability was assessed by comparison with untransfected cells treated with 1% Triton X-100 24 hours prior to FACS analysis. For primary NK cells, the cells were washed with 1X PBS and subsequently incubated in the dark at RT for 15 min with CD45-KrO (diluted 1:50) and CD56-APC-A750 (diluted 1:25) antibodies. The volume was then added up to 200 μL/well with 1X PBS and 7-AAD (final dilution 1:500) and immediately measured with the same FACS system. For primary NK cells, viability was assessed by comparison to cells heated at 95 °C for 1 min followed by 5 min incubation on ice. All FACS data was analyzed with FlowLogic 7.3 software. Gating strategy for primary NK cells can be observed in Figure S8; for KHYG-1 gating, see Figure S9. Gates were determined based on "dead" cells (treated with 1% Triton X-100 or heat) for viability, untransfected cells for baseline (auto)fluorescence, and unstained cells (with PBS incubation instead of CD45-KrO & CD56-APC-A750) for NK cell identification.

### 5.4.5 Confocal Live Cell Imaging

For visualization of (intracellular) eGFP expression, cells were imaged with the high content confocal fluorescent microscope Yokogawa Cell Voyager CV7000s (Tokyo, Japan). After 24-hour incubation with LNPs or following electroporation, cells were washed twice with 1X PBS and then incubated in the dark with Hoescht 33342 (diluted 1:500 as per manufacturer's protocol) at 37 °C for 10 min to stain cell nuclei, followed by fluorescent imaging. Images were analyzed with Columbus™ Image Data Storage and Analysis system.

## 5.5 Characterization & Analysis

### 5.5.1 Nuclear Magnetic Resonance (NMR) Spectroscopy

^{1}H NMR (400 MHz) spectra of polymers and their intermediates were measured on an Agilent 400-MR NMR spectrometer (Agilent Technologies, Santa Clara, USA). The residual solvent peak of $CDCl_3$ ($\delta$ = 7.26 ppm), DMSO-$d_6$ ($\delta$ = 2.50 ppm) or $D_2O$ ($\delta$ = 4.79 ppm) was used to calibrate chemical shifts. All spectra were analysed using MestReNova Software version 14.2.1-27684.

### 5.5.2 Gel Permeation Chromatography (GPC)

For polymer characterization, GPC was performed using two linked PLgel 5 μm mixed-D columns (Polymer Laboratories, UK) on an Alliance 2695 (Waters, the Netherlands) chromatography system, with column temperature set to 65 °C, coupled to a refractive index detector. DMF containing 10 mM LiCl was used as eluent at a rate of 1 mL/min. The sample concentration employed was 3 mg/mL and narrow defined PEG polymers (PSS, Germany) were used as calibration standards. Recording of data and calculations of molecular weights were done with Waters Empower 32 software.

### 5.5.3 High-Performance Liquid Chromatography (HPLC)

Reverse-phase HPLC analyses of peptides and chemical compounds (i.e., PUBAP intermediate) was conducted using an HPLC gradient system (Waters e2795 separations module) with UV detection (210 nm and 254nm). For chemicals analysis, it was equipped with a XBridge C18 column (Waters, 5 μm, 4.6 mm X

150mm) at RT. The gradient ran with a flow of 1 mL/min starting with Solvent A (0.1% FA, 5% ACN in water) to Solvent B (0.1% FA in ACN) within a timeframe of 20 mins, running a total period of 27 mins. The GALA-CG peptide was analyzed in a basic system (10 mM $NH_4HCO_3$ instead of 0.1% FA) on a TSKgel® G2000SWXL Column (Tosoh 08540, 7.8 mm X 300 mm) with identical elution settings. Recording of data and calculations of molecular weights were done with Waters Empower 32 software.

### 5.5.4 Agarose Gel Retardation Assay

Polyplexes were prepared as described above and diluted with HEPES buffer to a final mRNA concentration of 20 µg/mL. Polyplex solutions were split into 2 x 20 µL aliquots, of which one was mixed with 2 µL heparin sodium salt solution (25 mg/mL). Next, all samples, together with a sample containing only 20 µg/mL mRNA in 20 mM HEPES buffer (pH 7.4), were incubated at 37 °C for 45 mins and subsequently mixed with 4 µL of 6× Orange DNA loading dye. These samples were loaded into a 0.7% agarose gel containing Midori Green in tris-acetate-EDTA (TAE) buffer and the gel was run at 120 V for 20 mins before analysis by a ChemiDoc™ Imager (Bio-Rad Laboratories Inc., Hercules, CA) using Image Lab software (version 6.0.1). To test potential polyplex-destabilizing properties of various peptides, the same procedure was followed with the omission of heparin addition to part of the samples. Instead, the 20 µL polyplex solutions were supplemented with either no peptide (control), CM18-PTD4, INF7 or GALA-CG at a final concentration of 20 µM peptide, and incubated at RT for 2 hours before loading dye addition and agarose gel analysis.

### 5.5.5 Dynamic Light Scattering (DLS) & Zeta-Potential

Polyplexes and LNPs were characterized for size (diameter) and polydispersity index (PDI), by means of Dynamic Light Scattering (DLS) using a Zetasizer Nano-S at a 90° angle (Malvern Instruments, Worcestershire, UK), as well as zeta-potential using a Zetasizer Nano-Z (Malvern Instruments, Worcestershire, UK). For polyplexes, samples were prepared as described above and diluted to a final mRNA concentration of 5 µg/mL with 20 mM HEPES buffer (pH 7.4) just before DLS and zeta-potential measurement. For LNPs, 200 µL were diluted in 1X PBS (pH 7.4) up to a total volume of 500 µL for DLS and up to 700 µL for zeta-potential (typically dilutions between 5-70 times).

### 5.5.6 Encapsulation Efficiency (EE%)

Encapsulation efficiency (EE%) of mRNA for the LNP formulations was measured using the Quant-iT™ RiboGreen™ RNA Assay Kit for optimization experiments, and the Qubit™ RNA BR Assay Kit for electroporation-comparison experiments. Both were used according to manufacturer protocol; comparable results were observed for both assays. Briefly, mRNA-LNP formulations were first 50 times diluted with Tris-EDTA (pH 8.0) buffer in the presence or absence of 0.5% Triton X-100, and subsequently diluted 2 times with Qubit™ or Quant-iT™ assay reagent for 10 min incubation at RT. Fluorescent intensity was measured in a black 96-well plate using a Jasco FP-8300 spectrophotometer (excitation/emission: 644/673 nm for Qubit™, 485/530 nm for Quant-iT™). The unencapsulated mRNA concentration (free mRNA) was calculated from LNP samples incubated without Triton X-100. The total mRNA concentration (total mRNA), being both encapsulated and free mRNA, was determined from LNPs lysed with Triton X-100. To determine the EE%, the following formula was used: *EE% = ((total mRNA-free mRNA)/total mRNA) x 100%.* All samples were measured in triplicate, from which the mean EE% was calculated.

### 5.5.7 Statistical Analysis

Results were analyzed and illustrated using GraphPad Prism v7.0. Comparisons between experimental groups were analyzed by a two-tailed unpaired Student's *t* test, where $p < 0.05$ was considered statistically significant.

# 6. Acknowledgements

# 7. References

1. Johnson DB, Nebhan CA, Moslehi JJ, Balko JM. Immune-checkpoint inhibitors: long-term implications of toxicity. *Nat Rev Clin Oncol*. 2022;19(4):254-267. doi:10.1038/s41571-022-00600-w

2. Luke JJ, Flaherty KT, Ribas A, Long G v. Targeted agents and immunotherapies: Optimizing outcomes in melanoma. *Nat Rev Clin Oncol*. 2017;14(8):463-482. doi:10.1038/nrclinonc.2017.43

3. Mayor M, Yang N, Sterman D, Jones DR, Adusumilli PS. Immunotherapy for non-small cell lung cancer: Current concepts and clinical trials. *European Journal of Cardio-thoracic Surgery*. 2016;49(5):1324-1333. doi:10.1093/ejcts/ezv371

4. Rohaan MW, Wilgenhof S, Haanen JBAG. Adoptive cellular therapies: the current landscape. *Virchows Archiv*. 2019;474(4):449-461. doi:10.1007/s00428-018-2484-0

5. Myers JA, Miller JS. Exploring the NK cell platform for cancer immunotherapy. *Nat Rev Clin Oncol*. 2021;18(2):85-100. doi:10.1038/s41571-020-0426-7

6. Fang F, Xiao W, Tian Z. NK cell-based immunotherapy for cancer. *Semin Immunol*. 2017;31:37-54. doi:10.1016/j.smim.2017.07.009

7. Ingegnere T, Mariotti FR, Pelosi A, et al. Human CAR NK cells: A new non-viral method allowing high efficient transfection and strong tumor cell killing. *Front Immunol*. 2019;10(APR). doi:10.3389/fimmu.2019.00957

8. Prager I, Liesche C, van Ooijen H, et al. NK cells switch from granzyme B to death receptor-mediated cytotoxicity during serial killing. *Journal of Experimental Medicine*. 2019;216(9):2113-2127. doi:10.1084/jem.20181454

9. van Vliet AA, Georgoudaki AM, Raimo M, de Gruijl TD, Spanholtz J. Adoptive nk cell therapy: A promising treatment prospect for metastatic melanoma. *Cancers (Basel)*. 2021;13(18). doi:10.3390/cancers13184722

10. Bryceson YT, March ME, Ljunggren HG, Long EO. Activation, coactivation, and costimulation of resting human natural killer cells. *Immunol Rev*. 2006;214(1):73-91. doi:10.1111/j.1600-065X.2006.00457.x

11. Belizário JE, Neyra JM, Setúbal Destro Rodrigues MF. When and how NK cell-induced programmed cell death benefits immunological protection against intracellular pathogen infection. *Innate Immun*. 2018;24(8):452-465. doi:10.1177/1753425918800200

12. Koerner SP, André MC, Leibold JS, et al. An Fc-optimized CD133 antibody for induction of NK cell reactivity against myeloid leukemia. *Leukemia*. 2017;31(2):459-469. doi:10.1038/leu.2016.194

13. Castro F, Cardoso AP, Gonçalves RM, Serre K, Oliveira MJ. Interferon-gamma at the crossroads of tumor immune surveillance or evasion. *Front Immunol*. 2018;9(MAY). doi:10.3389/fimmu.2018.00847

14. Groh V, Rhinehart R, Secrist H, Bauer S, Grabstein KH, Spies T. Broad tumor-associated expression and recognition by tumor-derived T cells of MICA and MICB. *PNAS*. 1999;96:6879-6884. www.pnas.org.

15. Pende D, Rivera P, Marcenaro S, et al. Major Histocompatibility Complex Class I-related Chain A and UL16-Binding Protein Expression on Tumor Cell Lines of Different Histotypes: Analysis of Tumor Susceptibility to NKG2D-dependent Natural Killer Cell Cytotoxicity 1. *Cancer Res*. 2002;62:6178-6186. http://aacrjournals.org/cancerres/article-pdf/62/21/6178/2498539/ch2102006178.pdf

16. Cosman D, Jürgen M, Sutherland CL, et al. ULBPs, Novel MHC Class I-Related Molecules, Bind to CMV Glycoprotein UL16 and Stimulate NK Cytotoxicity through the NKG2D Receptor tions of most of the nonessential viral glycoproteins remain unknown. NK cells are also known to play an important role in c. *Immunity*. 2001;14:123-133.

17.    Raulet DH, Gasser S, Gowen BG, Deng W, Jung H. Regulation of ligands for the NKG2D activating receptor. *Annu Rev Immunol*. 2013;31:413-441. doi:10.1146/annurev-immunol-032712-095951

18.    Brandt CS, Baratin M, Yi EC, et al. The B7 family member B7-H6 is a tumor cell ligand for the activating natural killer cell receptor NKp30 in humans. *Journal of Experimental Medicine*. 2009;206(7):1495-1503. doi:10.1084/jem.20090681

19.    Pogge von Strandmann E, Simhadri VR, von Tresckow B, et al. Human Leukocyte Antigen-B-Associated Transcript 3 Is Released from Tumor Cells and Engages the NKp30 Receptor on Natural Killer Cells. *Immunity*. 2007;27(6):965-974. doi:10.1016/j.immuni.2007.10.010

20.    Gaggero S, Bruschi M, Petretto A, et al. Nidogen-1 is a novel extracellular ligand for the NKp44 activating receptor. *Oncoimmunology*. 2018;7(9). doi:10.1080/2162402X.2018.1470730

21.    Rosental B, Brusilovsky M, Hadad U, et al. Proliferating Cell Nuclear Antigen Is a Novel Inhibitory Ligand for the Natural Cytotoxicity Receptor NKp44. *The Journal of Immunology*. 2011;187(11):5693-5702. doi:10.4049/jimmunol.1102267

22.    Baychelier F, Sennepin A, Ermonval M, Dorgham K, Debre P, Vieillard V. Identification of a cellular ligand for the natural cytotoxicity receptor NKp44. *Blood*. 2013;122(17):2935-2942. doi:10.1182/blood-2013-03-489054

23.    Bernardini G, Antonangeli F, Bonanni V, Santoni A. Dysregulation of chemokine/chemokine receptor axes and NK cell tissue localization during diseases. *Front Immunol*. 2016;7(OCT). doi:10.3389/fimmu.2016.00402

24.    Parham P, Norman PJ, Abi-Rached L, Guethlein LA. Human-specific evolution of killer cell immunoglobulin-like receptor recognition of major histocompatibility complex class I molecules. *Philosophical Transactions of the Royal Society B: Biological Sciences*. 2012;367(1590):800-811. doi:10.1098/rstb.2011.0266

25.    Long EO. Negative signaling by inhibitory receptors: The NK cell paradigm. *Immunol Rev*. 2008;224(1):70-84. doi:10.1111/j.1600-065X.2008.00660.x

26.    Faure M, Long EO. KIR2DL4 (CD158d), an NK Cell-Activating Receptor with Inhibitory Potential. *The Journal of Immunology*. 2002;168(12):6208-6214. doi:10.4049/jimmunol.168.12.6208

27.    Karre K. NK Cells, MHC Class I Molecules and the Missing Self. *Scand J Immunol*. 2002;55:211-228.

28.    Majzner RG, Mackall CL. Tumor antigen escape from car t-cell therapy. *Cancer Discov*. 2018;8(10):1219-1226. doi:10.1158/2159-8290.CD-18-0442

29.    Ruella M, Maus M v. Catch me if you can: Leukemia Escape after CD19-Directed T Cell Immunotherapies. *Comput Struct Biotechnol J*. 2016;14:357-362. doi:10.1016/j.csbj.2016.09.003

30.    Kochenderfer JN, Dudley ME, Feldman SA, et al. B-cell depletion and remissions of malignancy along with cytokine-associated toxicity in a clinical trial of anti-CD19 chimeric-antigen-receptor-transduced T cells. *Blood*. 2012;119(12):2709-2720. doi:10.1182/blood-2011-10

31.    Depil S, Duchateau P, Grupp SA, Mufti G, Poirot L. 'Off-the-shelf' allogeneic CAR T cells: development and challenges. *Nat Rev Drug Discov*. 2020;19(3):185-199. doi:10.1038/s41573-019-0051-2

32.    Hay KA. Cytokine release syndrome and neurotoxicity after CD19 chimeric antigen receptor-modified (CAR-) T cell therapy. *Br J Haematol*. 2018;183(3):364-374. doi:10.1111/bjh.15644

33.    Olson JA, Leveson-Gower DB, Gill S, Baker J, Beilhack A, Negrin RS. NK cells mediate reduction of GVHD by inhibiting activated, alloreactive T cells while retaining GVT effects. *Blood*. 2010;115(21):4293-4301. doi:10.1182/blood-2009-05-222190

34.    Shaffer BC, le Luduec JB, Forlenza C, et al. Phase II Study of Haploidentical Natural Killer Cell Infusion for Treatment of Relapsed or Persistent Myeloid Malignancies Following Allogeneic Hematopoietic Cell Transplantation. *Biology of Blood and Marrow Transplantation*. 2016;22(4):705-709. doi:10.1016/j.bbmt.2015.12.028

35. Passweg JR, Tichelli A, Meyer-Monard S, et al. Purified donor NK-lymphocyte infusion to consolidate engraftment after haploidentical stem cell transplantation. *Leukemia*. 2004;18(11):1835-1838. doi:10.1038/sj.leu.2403524

36. Ruggeri L, Capanni M, Urbani E, et al. Effectiveness of Donor Natural Killer Cell Alloreactivity in Mismatched Hematopoietic Transplants. *Science (1979)*. 2002;295:2097-2100.

37. Liu E, Marin D, Banerjee P, et al. Use of CAR-Transduced Natural Killer Cells in CD19-Positive Lymphoid Tumors. *New England Journal of Medicine*. 2020;382(6):545-553. doi:10.1056/nejmoa1910607

38. Dolstra H, Roeven MWH, Spanholtz J, et al. Successful transfer of umbilical cord blood CD34+ hematopoietic stem and progenitor-derived NK cells in older acute myeloid leukemia patients. *Clinical Cancer Research*. 2017;23(15):4107-4118. doi:10.1158/1078-0432.CCR-16-2981

39. Carlsten M, Levy E, Karambelkar A, et al. Efficient mRNA-based genetic engineering of human NK cells with high-affinity CD16 and CCR7 augments rituximab-induced ADCC against lymphoma and targets NK cell migration toward the lymph node-associated chemokine CCL19. *Front Immunol*. 2016;7(MAR). doi:10.3389/fimmu.2016.00105

40. Carlsten M, Childs RW. Genetic manipulation of NK cells for cancer immunotherapy: Techniques and clinical implications. *Front Immunol*. 2015;6(JUN). doi:10.3389/fimmu.2015.00266

41. Kennedy PR, Felices M, Miller JS. Challenges to the broad application of allogeneic natural killer cell immunotherapy of cancer. *Stem Cell Res Ther*. 2022;13(1):1-13. doi:10.1186/s13287-022-02769-4

42. Robbins GM, Wang M, Pomeroy EJ, Moriarity BS. Nonviral genome engineering of natural killer cells. *Stem Cell Res Ther*. 2021;12(1). doi:10.1186/s13287-021-02406-6

43. Mantesso S, Geerts D, Spanholtz J, Kučerová L. Genetic Engineering of Natural Killer Cells for Enhanced Antitumor Function. *Front Immunol*. 2020;11. doi:10.3389/fimmu.2020.607131

44. Wilk AJ, Weidenbacher NLB, Vergara R, et al. Charge-altering releasable transporters enable phenotypic manipulation of natural killer cells for cancer immunotherapy. *Blood Adv*. 2020;4(17):4244-4255. doi:10.1182/BLOODADVANCES.2020002355

45. Wilk AJ, Benner NL, Vergara R, et al. Charge-Altering Release Transporters Enable Specific Phenotypic Manipulation of REsting Primary Natural Killer Cells. *bioRxiv*. Published online 2020. doi:10.1101/2020.02.28.970491

46. Mitchell MJ, Billingsley MM, Haley RM, Wechsler ME, Peppas NA, Langer R. Engineering precision nanoparticles for drug delivery. *Nat Rev Drug Discov*. 2021;20(2):101-124. doi:10.1038/s41573-020-0090-8

47. Polack FP, Thomas SJ, Kitchin N, et al. Safety and Efficacy of the BNT162b2 mRNA Covid-19 Vaccine. *New England Journal of Medicine*. 2020;383(27):2603-2615. doi:10.1056/nejmoa2034577

48. Ita K. Polyplexes for gene and nucleic acid delivery: Progress and bottlenecks. *European Journal of Pharmaceutical Sciences*. 2020;150. doi:10.1016/j.ejps.2020.105358

49. Lou B, de Koker S, Lau CYJ, Hennink WE, Mastrobattista E. MRNA Polyplexes with Post-Conjugated GALA Peptides Efficiently Target, Transfect, and Activate Antigen Presenting Cells. *Bioconjug Chem*. 2018;30(2):461-475. doi:10.1021/acs.bioconjchem.8b00524

50. Fröhlich E. The role of surface charge in cellular uptake and cytotoxicity of medical nanoparticles. *Int J Nanomedicine*. 2012;7:5577-5591. doi:10.2147/IJN.S36111

51. Lou B, de Beuckelaer A, Dakwar GR, et al. Post-PEGylated and crosslinked polymeric ssRNA nanocomplexes as adjuvants targeting lymph nodes with increased cytolytic T cell inducing properties. *Journal of Controlled Release*. 2018;284:73-83. doi:10.1016/j.jconrel.2018.06.010

52. Luten J, Akeroyd N, Funhoff A, Lok MC, Talsma H, Hennink WE. Methacrylamide polymers with hydrolysis-sensitive cationic side groups as degradable gene carriers. *Bioconjug Chem*. 2006;17(4):1077-1084. doi:10.1021/bc060068p

53. Bus T, Traeger A, Schubert US. The great escape: how cationic polyplexes overcome the endosomal barrier. *J MaterChemB*. 2018;6(43):6904-6918.

54. Baden LR, el Sahly HM, Essink B, et al. Efficacy and Safety of the mRNA-1273 SARS-CoV-2 Vaccine. *New England Journal of Medicine*. 2021;384(5):403-416. doi:10.1056/nejmoa2035389

55. Voysey M, Clemens SAC, Madhi SA, et al. Safety and efficacy of the ChAdOx1 nCoV-19 vaccine (AZD1222) against SARS-CoV-2: an interim analysis of four randomised controlled trials in Brazil, South Africa, and the UK. *The Lancet*. 2021;397(10269):99-111. doi:10.1016/S0140-6736(20)32661-1

56. Hou X, Zaks T, Langer R, Dong Y. Lipid nanoparticles for mRNA delivery. *Nat Rev Mater*. 2021;6(12):1078-1094. doi:10.1038/s41578-021-00358-0

57. Buschmann M, Carrasco M, Alishetty S, Paige M, Alameh MG, Weissman D. Nanomaterial Delivery Systems for mRNA Vaccines. *Vaccines (Basel)*. 2021;9(65).

58. Hassett KJ, Higgins J, Woods A, et al. Impact of lipid nanoparticle size on mRNA vaccine immunogenicity. *Journal of Controlled Release*. 2021;335:237-246. doi:10.1016/j.jconrel.2021.05.021

59. Spadea A, Jackman M, Cui L, et al. Nucleic Acid-Loaded Lipid Nanoparticle Interactions with Model Endosomal Membranes. *ACS Appl Mater Interfaces*. 2022;14(26):30371-30384.

60. Maugeri M, Nawaz M, Papadimitriou A, et al. Linkage between endosomal escape of LNP-mRNA and loading into EVs for transport to other cells. *Nat Commun*. 2019;10:4333.

61. Cheng J, Tang X, Zhao J, Shi T, Zhao P, Lin C. Multifunctional cationic polyurethanes designed for non-viral cancer gene therapy. *Acta Biomater*. 2016;30:155-167. doi:10.1016/j.actbio.2015.11.048

62. Vaidyanathan S, Chen J, Orr B, Banaszak Holl M. Cationic Polymer Intercalation into the Lipid Membrane Enables Intact Polyplex DNA Escape from Endosomes for Gene Delivery. *Mol Pharmaceutics*. 2016;13(6):1967-1978.

63. Hanzlíková M, Ruponen M, Galli E, et al. Mechanisms of polyethylenimine-mediated DNA delivery: free carrier helps to overcome the barrier of cell-surface glycosaminoglycans. *Journal of Gene Medicine*. 2011;13(7-8):402-409. doi:10.1002/jgm.1587

64. Debus H, Baumhof P, Probst J, Kissel T. Delivery of messenger RNA using poly(ethylene imine)-poly(ethylene glycol)-copolymer blends for polyplex formation: Biophysical characterization and in vitro transfection properties. *Journal of Controlled Release*. 2010;148(3):334-343. doi:10.1016/j.jconrel.2010.09.007

65. Yagita M, Huang CL, Umehara H, et al. *A Novel Natural Killer Cell Line (KHYG-1) from a Patient with Aggressive Natural Killer Cell Leukemia Carrying a P53 Point Mutation*. Vol 14.; 2000. www.nature.com/leu

66. Gong JH, Maki G, Klingemann GH. Characterization of a human cell line (NK-92) with phenotypical and functional characteristics of activated natural killer cells. *Leukemia*. 1994;8(4):652-658.

67. Misra SK, Biswas J, Kondaiah P, Bhattacharya S. Gene Transfection in High Serum Levels: Case Studies with New Cholesterol Based Cationic Gemini Lipids. *PLoS One*. 2013;8(7). doi:10.1371/journal.pone.0068305

68. Pezzoli D, Giupponi E, Mantovani D, Candiani G. Size matters for in vitro gene delivery: Investigating the relationships among complexation protocol, transfection medium, size and sedimentation. *Sci Rep*. 2017;7(February):1-11. doi:10.1038/srep44134

69. Madani F, Lindberg S, Langel Ü, Futaki S, Gräslund A. Mechanisms of cellular uptake of cell-penetrating peptides. *Journal of Biophysics*. Published online 2011. doi:10.1155/2011/414729

70. Mastrobattista E, Koning GA, van Bloois L, Filipe ACS, Jiskoot W, Storm G. Functional characterization of an endosome-disruptive peptide and its application in cytosolic delivery of immunoliposome-entrapped proteins. *Journal of Biological Chemistry*. 2002;277(30):27135-27143. doi:10.1074/jbc.M200429200
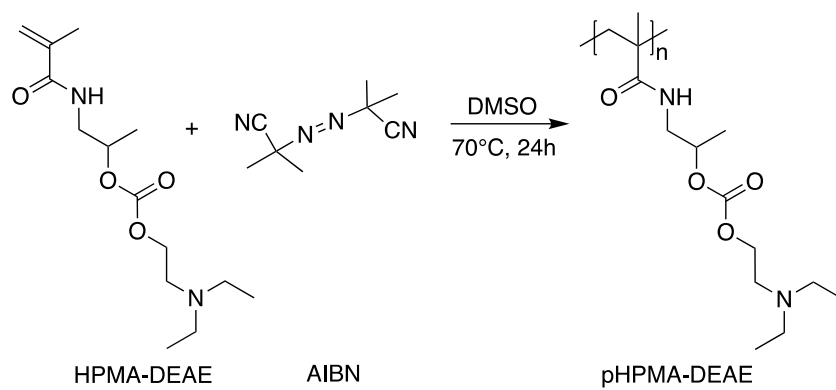
71. Schach DK, Rock W, Franz J, Bonn M, Parekh SH, Weidner T. Reversible Activation of a Cell-Penetrating Peptide in a Membrane Environment. *J Am Chem Soc*. 2015;137(38):12199-12202. doi:10.1021/jacs.5b06720

72. Han X, Bushweller J, Cafiso D, Tamm L. Membrane structure and fusion-triggeringconformational change of the fusion domainfrom influenza hemagglutinin. *Nat Struct Biol*. 2001;8(8):715-720.

73. Felgner PL, Ringold GM. Cationic liposome-mediated transfection. *Nature*. 1989;337:26-27.

74. Kichler A, Mason AJ, Bechinger B. Cationic amphipathic histidine-rich peptides for gene delivery. *Biochim Biophys Acta Biomembr*. 2006;1758(3):301-307. doi:10.1016/j.bbamem.2006.02.005

75. Kichler A, Leborgne C, März J, Danos O, Bechinger B. Histidine-rich amphipathic peptide antibiotics promote efficient delivery of DNA into mammalian cells. *PNAS*. 2003;100(4):1564-1568. www.pnas.orgcgidoi10.1073pnas.0337677100

76. El-Sayed A, Masuda T, Akita H, Harashima H. Stearylated INF7 peptide enhances endosomal escape and gene expression of PEGylated nanoparticles both in vitro and in vivo. *J Pharm Sci*. 2012;101(2):879-882. doi:10.1002/jps.22807

77. El-Sayed A, Masuda T, Khalil I, Akita H, Harashima H. Enhanced gene expression by a novel stearylated INF7 peptide derivative through fusion independent endosomal escape. *Journal of Controlled Release*. 2009;138(2):160-167. doi:10.1016/j.jconrel.2009.05.018

78. Hatakeyama H, Ito E, Akita H, et al. A pH-sensitive fusogenic peptide facilitates endosomal escape and greatly enhances the gene silencing of siRNA-containing nanoparticles in vitro and in vivo. *Journal of Controlled Release*. 2009;139(2):127-132. doi:10.1016/j.jconrel.2009.06.008

79. Simoes S, Slepushkin V, Gaspar R, Pedroso De Lima MC, Düzgünes N. *Gene Delivery by Negatively Charged Ternary Complexes of DNA, Cationic Liposomes and Transferrin or Fusigenic Peptides*. Vol 5.; 1998. http://www.stockton-press.co.uk/gt

80. Jones SW, Christison R, Bundell K, et al. Characterisation of cell-penetrating peptide-mediated peptide delivery. *Br J Pharmacol*. 2005;145(8):1093-1102. doi:10.1038/sj.bjp.0706279

81. Rittner K, Benavente A, Bompard-Sorlet A, et al. New basic membrane-destabilizing peptides for plasmid-based gene delivery in vitro and in vivo. *Molecular Therapy*. 2002;5(2):104-114. doi:10.1006/mthe.2002.0523

82. Akishiba M, Takeuchi T, Kawaguchi Y, et al. Cytosolic antibody delivery by lipid-sensitive endosomolytic peptide. *Nat Chem*. 2017;9(8):751-761. doi:10.1038/NCHEM.2779

83. Del'Guidice T, Lepetit-Stoffaes JP, Bordeleau LJ, et al. Membrane permeabilizing amphiphilic peptide delivers recombinant transcription factor and CRISPR-Cas9/Cpf1 ribonucleoproteins in hard-to-modify cells. *PLoS One*. 2018;13(4). doi:10.1371/journal.pone.0195558

84. Krishnamurthy S, Wohlford-Lenane C, Kandimalla S, et al. Engineered amphiphilic peptides enable delivery of proteins and CRISPR-associated nucleases to airway epithelia. *Nat Commun*. 2019;10(1):1-12. doi:10.1038/s41467-019-12922-y

85. Sabnis S, Kumarasinghe ES, Salerno T, et al. A Novel Amino Lipid Series for mRNA Delivery: Improved Endosomal Escape and Sustained Pharmacology and Safety in Non-human Primates. *Molecular Therapy*. 2018;26(6):1509-1519. doi:10.1016/j.ymthe.2018.03.010

86. Gilleron J, Querbes W, Zeigerer A, et al. Image-based analysis of lipid nanoparticle-mediated siRNA delivery, intracellular trafficking and endosomal escape. *Nat Biotechnol*. 2013;31(7):638-646. doi:10.1038/nbt.2612

87. Patel S, Ashwanikumar N, Robinson E, et al. Naturally-occurring cholesterol analogues in lipid nanoparticles induce polymorphic shape and enhance intracellular delivery of mRNA. *Nat Commun*. 2020;11(1). doi:10.1038/s41467-020-14527-2

88. Prabha S, Arya G, Chandra R, Ahmed B, Nimesh S. Effect of size on biological properties of nanoparticles employed in gene delivery. *Artif Cells Nanomed Biotechnol*. 2016;44(1):83-91. doi:10.3109/21691401.2014.913054

89. Ryals RC, Patel S, Acosta C, McKinney M, Pennesi ME, Sahay G. The effects of PEGylation on LNP based mRNA delivery to the eye. *PLoS One*. 2020;15(10 October). doi:10.1371/journal.pone.0241006

90. Song LY, Ahkong QF, Rong Q, et al. Characterization of the inhibitory effect of PEG-lipid conjugates on the intracellular delivery of plasmid and antisense DNA mediated by cationic lipid liposomes. *Biochim Biophys Acta*. 2002;1558(1):1-13. doi:10.1016/S0005-2736(01)00399-6

91. Okuda K, Sato Y, Iwakawa K, et al. On the size-regulation of RNA-loaded lipid nanoparticles synthesized by microfluidic device. *Journal of Controlled Release*. 2022;348:648-659. doi:10.1016/j.jconrel.2022.06.017

92. Operti MC, Dölen Y, Keulen J, van Dinther EAW, Figdor CG, Tagit O. Microfluidics-assisted size tuning and biological evaluation of PLGA particles. *Pharmaceutics*. 2019;11(11). doi:10.3390/pharmaceutics11110590

93. Batista Napotnik T, Polajžer T, Miklavčič D. Cell death due to electroporation – A review. *Bioelectrochemistry*. 2021;141. doi:10.1016/j.bioelechem.2021.107871

94. Morotomi-Yano K, Yano KI. Calcium-dependent activation of transglutaminase 2 by nanosecond pulsed electric fields. *FEBS Open Bio*. 2017;7(7):934-943. doi:10.1002/2211-5463.12227

95. Morotomi-Yano K, Oyadomari S, Akiyama H, Yano K ichi. Nanosecond pulsed electric fields act as a novel cellular stress that induces translational suppression accompanied by eIF2α phosphorylation and 4E-BP1 dephosphorylation. *Exp Cell Res*. 2012;318(14):1733-1744. doi:10.1016/j.yexcr.2012.04.016

96. Stapulionis R. Electric pulse-induced precipitation of biological macromolecules in electroporation. *Bioelectrochemistry and Bioenergetics*. 1999;48(1):249-254. doi:10.1016/S0302-4598(98)00206-2

97. Kooijmans SAA, Stremersch S, Braeckmans K, et al. Electroporation-induced siRNA precipitation obscures the efficiency of siRNA loading into extracellular vesicles. *Journal of Controlled Release*. 2013;172(1):229-238. doi:10.1016/j.jconrel.2013.08.014

98. Breslow R, Huang DL. Effects of metal ions, including Mg2+ and lanthanides, on the cleavage of ribonucleotides and RNA model compounds. *Proc Natl Acad Sci U S A*. 1991;88(10):4080-4083. doi:10.1073/pnas.88.10.4080

99. Li B, Luo X, Dong Y. Effects of Chemically Modified Messenger RNA on Protein Expression. *Bioconjug Chem*. 2016;27(3):849-853. doi:10.1021/acs.bioconjchem.6b00090
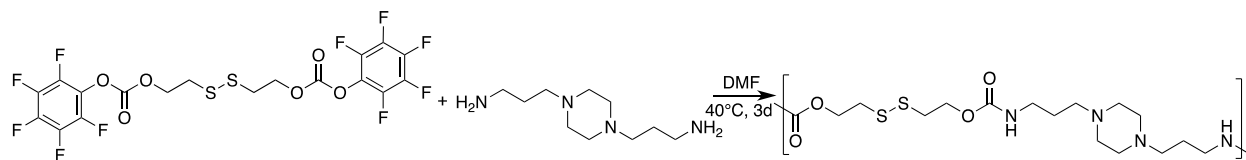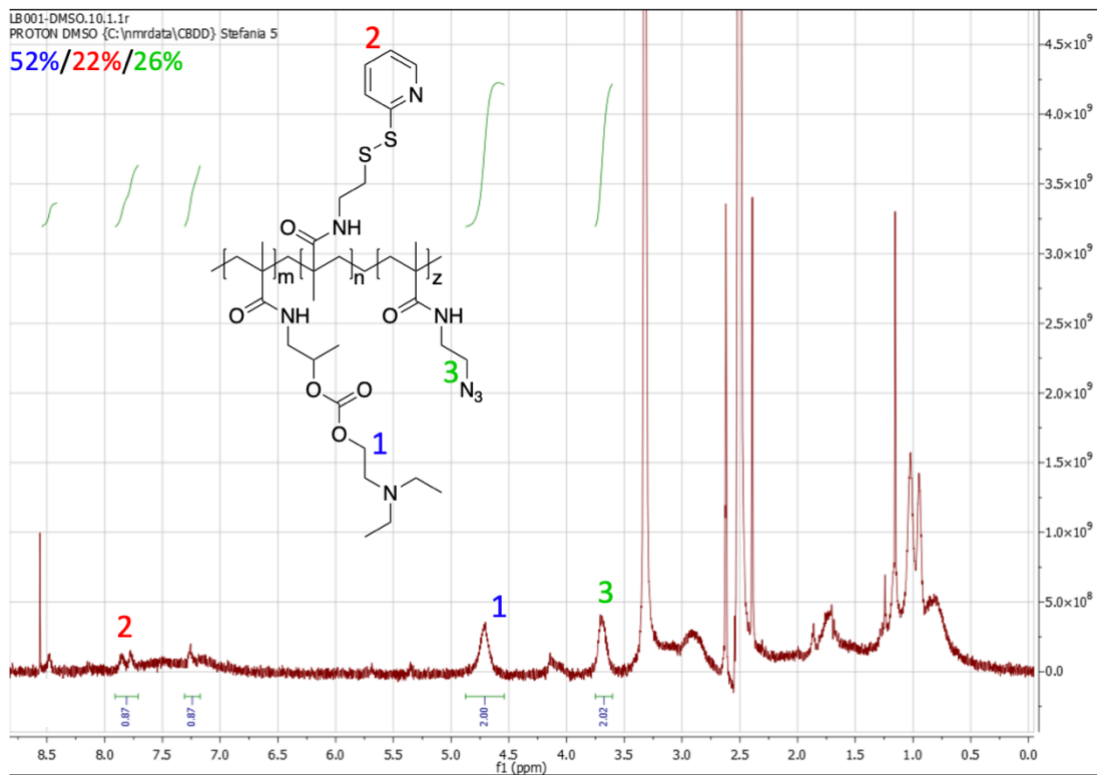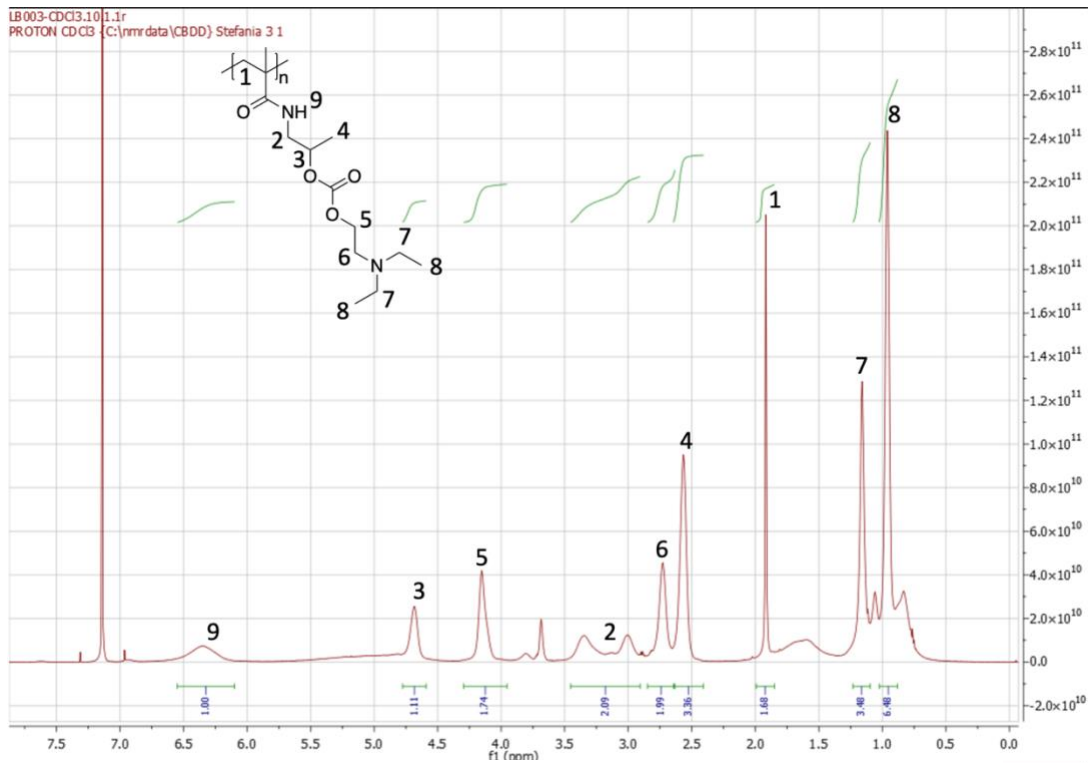
# Supplementary
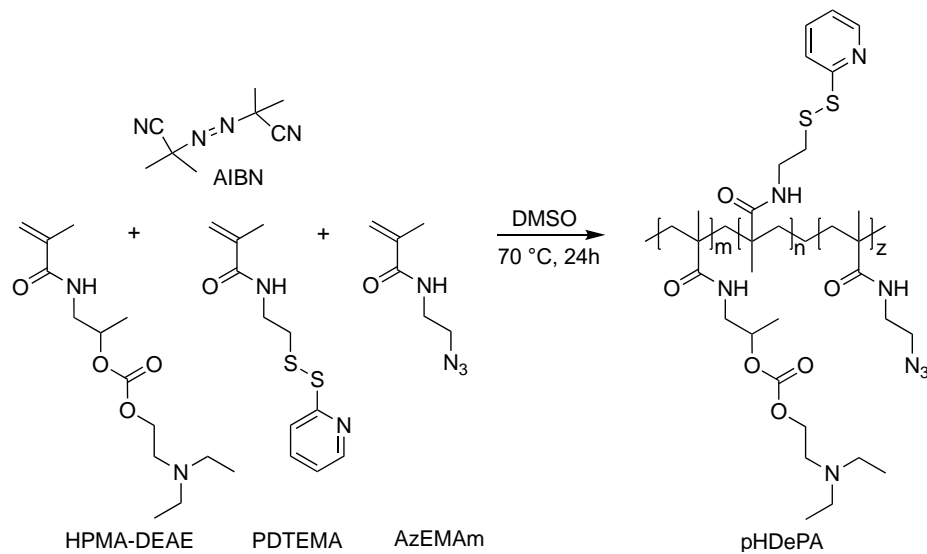


*Scheme S1. pHDePA synthesis.*



*Scheme S2. pHPMA-DEAE synthesis.*



*Scheme S3. PUBAP synthesis.*

*Figure S1. $^1H$ NMR of HPMA-DEAE in CDCl$_3$.*



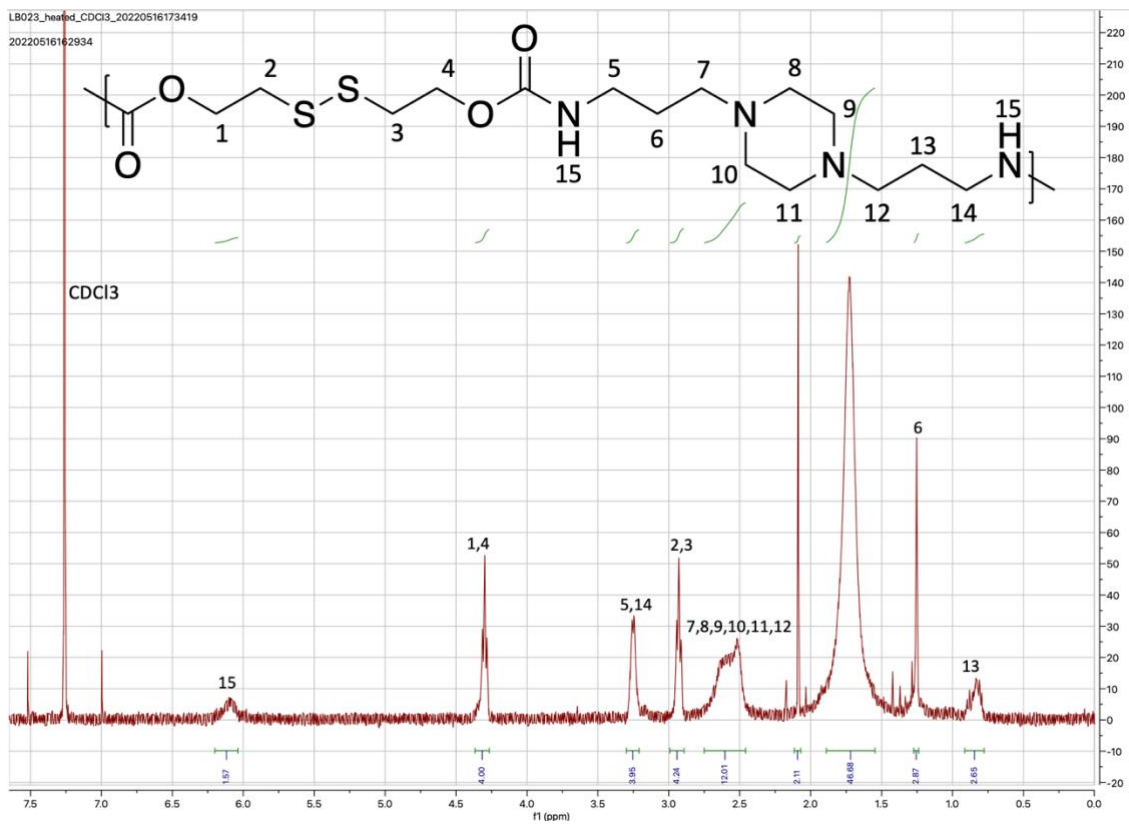*Figure S2. $^1H$ NMR of pHDePA in DMSO to assess monomer ratio.*

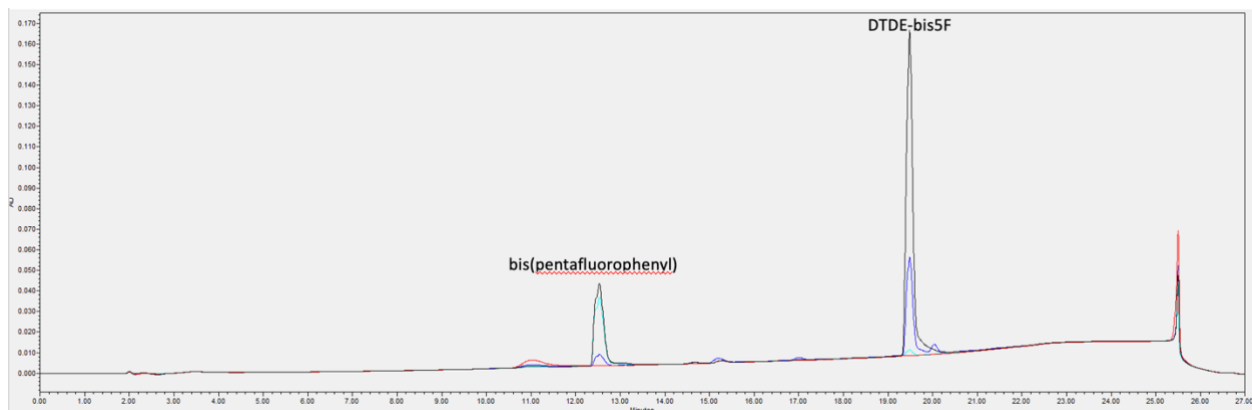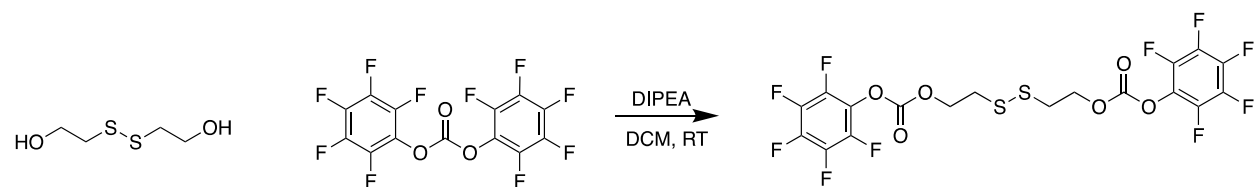*Figure S3. $^1H$ NMR of PUBAP in CDCl$_3$.*



*Figure S4. PUBAP intermediate DTDE-bis5F on HPLC (black chromatogram), showing residual bis(pentafluorophenyl) presence.*
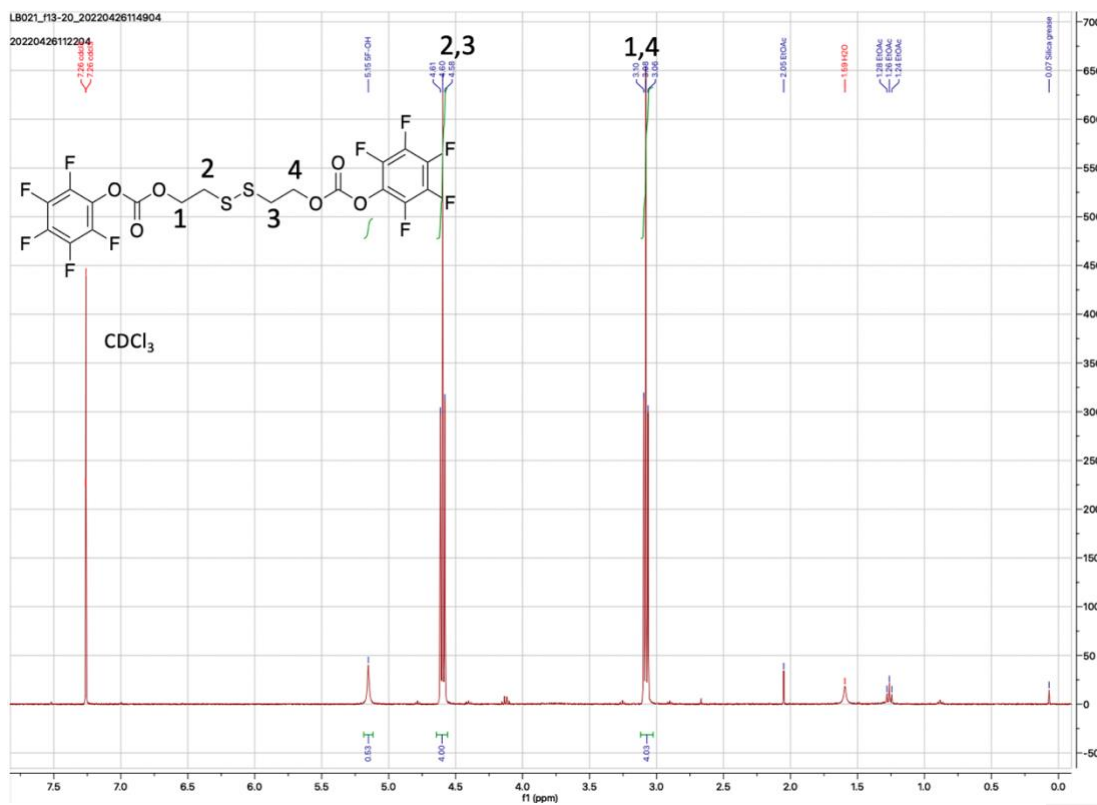
Scheme S4. DTDE-bis5F synthesis.



Figure S5. $^1$H NMR of DTDE-bis5F in CDCl$_3$.

Table S1. Free polymer zeta-potential.

| Polyplex | ζ-potential (mV ± SD)[a] | Buffer |
|---|---|---|
| PUBAP | +22.23 ± 0.50 | 20 mM HEPES, pH 7.4 |
| pHDePA | +16.40 ± 0.95 | 20mM ammonium acetate pH 5.0 |
| pHPMA-DEAE | +21.60 ± 0.98 | 20mM ammonium acetate pH 5.0 |

[a]Determined by Zetasizer.
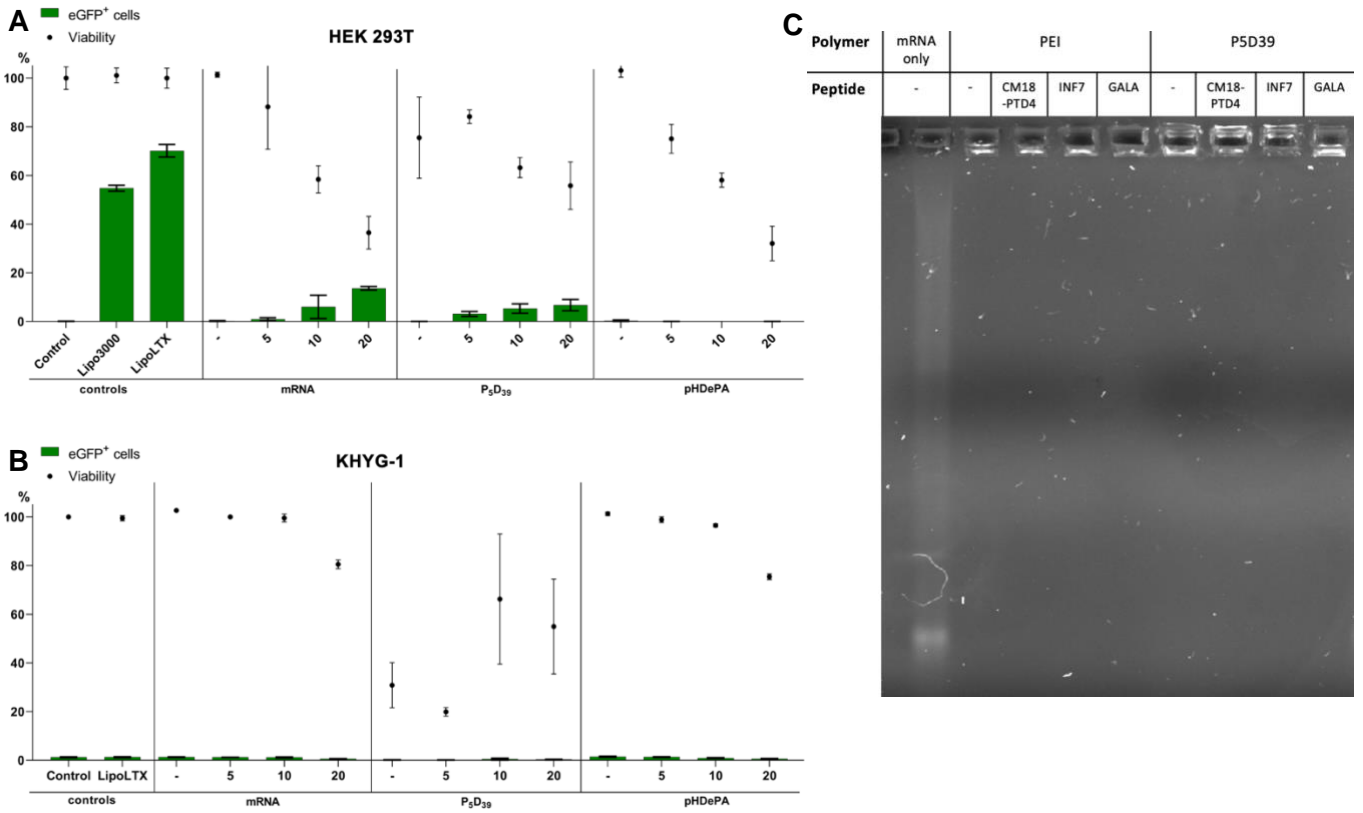


Figure S6. Transfection rates and viability of (A) HEK 293T cells and (B) KHYG-1 cells after 24 hour incubation with polyplexes combined with a concentration range of LAH5 peptide. (C) Agarose gel retardation assay with peptide-polyplex combination.
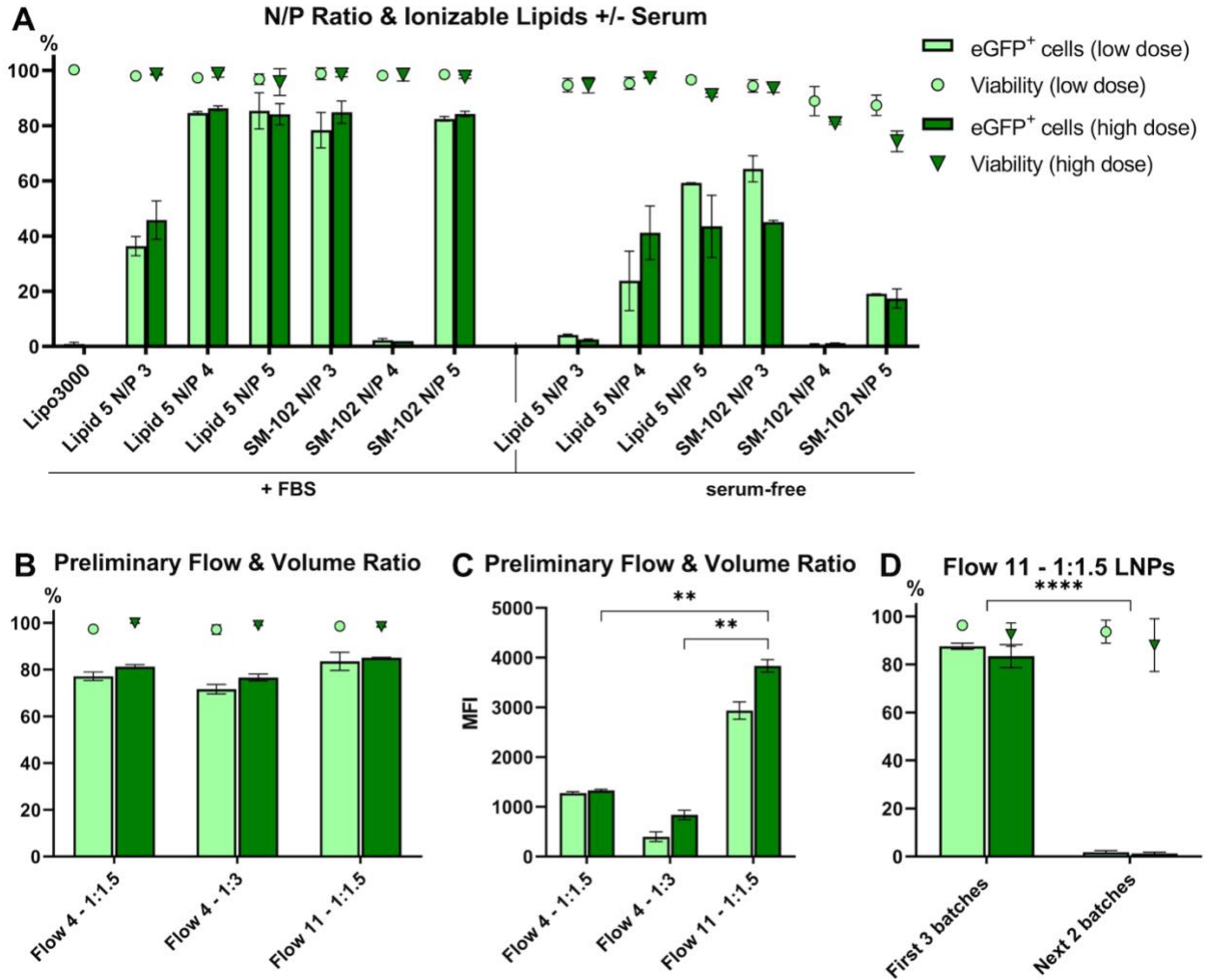
*Figure S7. Transfection optimizations in KHYG-1 cells. (**A**) LNP-based transfection with Lipid 5 and SM-102 in the presence and absence of fetal bovine serum (FBS). (**B**) Preliminary microfluidic optimizations in LNPs prepared with cholesterol (instead of β-sitosterol) presented as percentage of eGFP positive cells and viability, and (**C**) MFI values. (**D**) β-Sitosterol-containing LNPs prepared at 11 mL/min and 1:1.5 lipid:mRNA ratio showing loss of transfection efficiency after three successful batches. \*\*p<0.01, \*\*\*\*p<0.0001.*
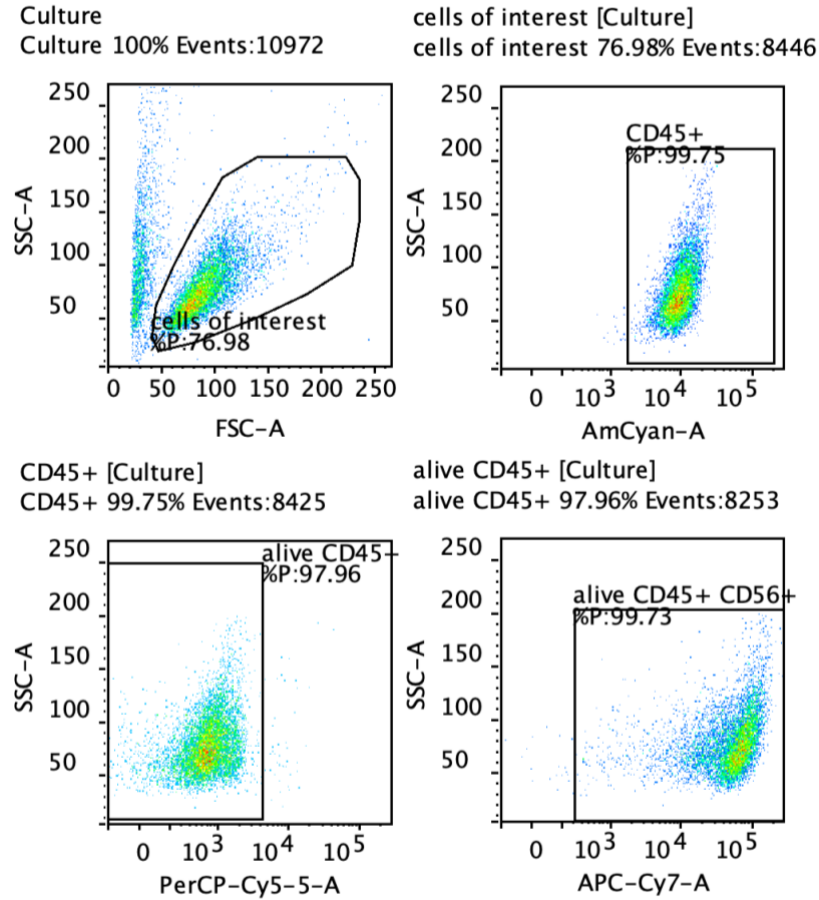
*Figure S8. Primary NK cell gating. From top left to bottom right: gating of single cells, gating of CD45 positive cells, gating of alive CD45 positive cells, gating of CD56 positive CD45 positive alive cells.*
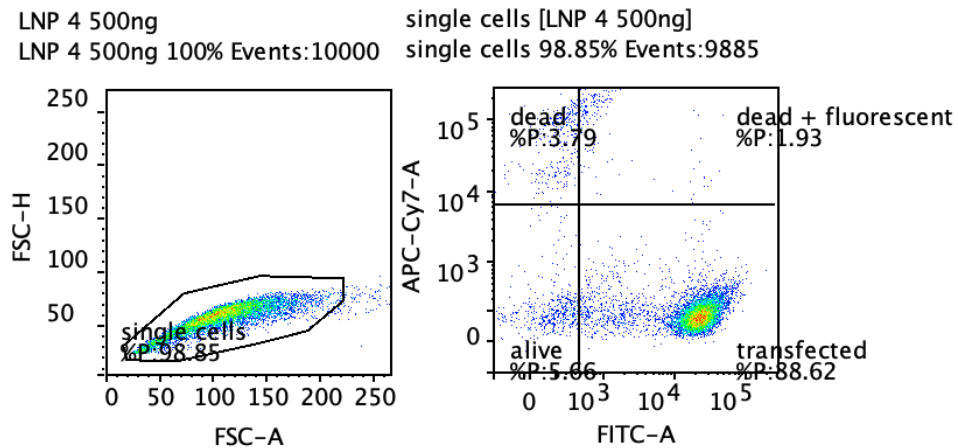


*Figure S9. KHYG-1 cell gating. Single cells are first gated (left panel), followed by fluorescence & viability gating (FITC-A & APC-Cy7-A, respectively; right panel) based on untransfected and dead controls. The reported percentage of transfected cells is based on the quadrant labeled "transfected" and hence encompasses only viable cells.*